Treball Fi de Màster

Màster Universitari en Enginyeria Química

Graft copolymers with a random distribution of pyrrole monomer with hydrophilic functionalities

MEMÒRIA

Autor: Brenda Guadalupe Molina García

Director: Elaine Armelin Diggroc

Convocatòria: Setembre 2016

ETSEIB

Escola Tècnica Superior
d'Enginyeria Industrial de Barcelona

UPC

Abstract

An electroactive biomaterial was obtained from the electropolymerization of pyrrole (Py) monomer and a macromonomer called PAB53, which has pyrrole as backbone and chains of PEG_{2000} grafted. The copolymerization was carried out at a molar ratio of 1:1 of Py:PAB53 and at three polymerization times (300, 500 and 1000s), resulting in films with cauliflower-like structures as surface morphology in all cases. The topography, thickness and wettability increased proportionally to the polymerization time, attributed to higher concentrations of PAB53 in the resulting copolymer films. Therefore, the increase of PEG chains, which favors the formation of valleys and hills in the surface morphology, is also responsible for a higher hydrophilicity in the copolymer films. The electroactivity of the compounds were affected negatively with the incorporation on the PEG. However, the optical and conductive properties were good, showing a similar band gap than the semiconductor PPy homopolymer.

It was established that the best film was the copolymer P(Py-*co*-PAB53) generated at 1000s, which was found to be an active surface for adsorption of BSA and Lyz proteins, the results revealed that the affinity of this copolymer is higher than the PPy homopolymer, suggesting that it is a promising polymer for bioengineering applications.

Table of contents

Index of Tables

Index of Figures

Glossary

AFM	Atomic force microscopy
Ag|AgCl	Silver|silver chloride
AzbPy	Azomethine-containig bis-pyrrole monomer
$BaSO_4$	Barium sulfate
BME	Basal medium eagle
BSA	Bovine serum albumin
CA	Chronoamperometry
CPs	Conducting polymers
CV	Cyclic voltammetry
EAPs	Electroactive polymers
FTIR	Fourier Transform Infra-red Spectroscopy
H-RMN	Proton nuclear magnetic resonance
ITO	Indium-tin oxide
KBr	Potassium bromide
KCl	Potassium chloride
LEA	Loss of electroactivity
$LiClO_4$	Lithium perchlorate
Lyz	Lysozyme from chicken egg white
P(Py-*co*-PAB53)	Copolymer of PPy and a macromonomer PAB53

PAB53	AzbPy-*g*-PEG macromonomer
PAni	Polyaniline
PCL	Polycaprolactone
PEG_{2000}	Poly(ethylene glycol) with a molecular weight of 2000 g/mol
PEO	Polyethylene oxide
PGA	Poly(glycolic acid)
PLA	Poly(lactic acid)
PNCPy	Poly(*N*-cyanoethylpyrrole)
PNMPy	Poly(*N*-methypyrrole)
PPE	Poly(phenylene ethynylene) (PPE)
PPP	Poly(*p*-phenylene)
PPV	Poly(*p*-phenylene vinylene)
PPy	Polypyrrole
PTh	Polythiophene
Py	Pyrrole
SDS	Sodium dodecyl sulfate
SEM	Scanning electron microscopy
TEMED	Tetramethylethylenediamine
t_{pol}	Polymerization time
Tris	Tris(hydroximethyl) aminomethane o 2-Amino-2-hidroximetil-propano-1,3-dio buffer

UV-Vis	Ultraviolet–visible spectroscopy
WCA	Water contact angle

Symbols

ΔQ	Difference between the oxidation charge (C) of the second and the last cycle
$\mathbf{Q_I}$	Oxidation charge corresponding to the first cycle (C)
$\boldsymbol{A_{\lambda max}}$	Absorbance in wavelength (nm)
$\boldsymbol{E_g}$	Band gap energy (eV)
$\boldsymbol{h}$	Planck constant (6.6261×10^{-34} J·s)
$\boldsymbol{f}$	Frequency (Hz)
$\boldsymbol{\lambda}$	Wavelength (nm)
$\boldsymbol{c}$	Speed of light in vacuum (approximately 3.00×10^{8} m/s).

1. Introduction

In the last three decades, conventional materials such as metals and alloys are being replaced by polymers thanks to their attractive properties compared to inorganic materials. They are easily processed and manufactured, lightweight, inexpensive, fracture tolerant and pliable [1], all this properties make them useful in many areas such as construction, packaging, transport, agriculture. Additionally, they are employed in new technologies like electronics, computer, communications, image, sound and in the diagnostic and treatment of many diseases.

The development of plastic in the 30s, 40s and 50s enabled the progress of medical devices that overtook and eventually replaced the foundation material with newer and better materials. New polymeric material developments continued to allow a virtual explosion of devices and implements, which were able to rely on the excellent properties that are offered by engineering polymers. Moreover, not only the devices industry is growing up, also the health-care industry, providing treatments to a great segment of the overall population, thanks to the rise of synthetic biodegradable and biocompatible polymers [2].

In order to continue with the developed of new and beneficial materials, the structure and topology of polymers have been modified, changing their mechanical, electrical and thermal properties.

Recently, polymeric materials with “intelligence” at molecular level are being developed, for example, polymers that respond to external stimuli like an electrical field, pH, a magnetic field, and light. These intelligent polymers are called active polymers and, due to a variety of stimuli, there are many types of active polymers but depending on the type of actuation they are classified as: (i) non-electrically deformable polymers (actuated by non-electric stimuli such as pH, light, temperature, etc.) and (ii) electroactive polymers (EAPs) (actuated by electrical inputs) [1] [3].

1.1. Electroactive Polymers (EAPs)

EAPs have been amply studied and are classified according to the mode of their electric transport. One group includes polymers having transport almost exclusively of the ionic type, often called *polymer electrolytes* or *polymer ionic*. The other group includes polymeric materials where the transport mechanism is mainly electronic in nature and which are commonly termed *conducting polymers (CPs)* [4].

The difference between ionic and electronic EAPs is the necessary driving system. Ionic EAPs require low voltages for actuation, typically 1V or less, but they consume relatively large current (10^2 mA to ampere range). On the other hand, electronic EAPs operate at high voltages up to a few kV, and consume small current whose order is of μA [5]. Also, the electronic properties of ionic materials are substantially different from those of electronic materials. Ionic material are more closely related to conductors with the important exception that an ionic material is conducting charged atoms or molecules, whereas an electronic conductor is conducting electrons [6].

The conducting polymers research starts in 1977 when Alan J. Heeger, Allan G. MacDiarmid and Hideki Shirakawa found that some organic materials, like polyacetylene, can be made conductive almost like a metal [7]. Before their work, organic polymers were considered as insulating materials but this discovery converted them into materials with interesting properties because they combine the characteristic of a conventional plastic (low production cost, low density, good mechanical properties,…) with the capacity of conduct electricity.

Therefore, the discovery of a new class of organic polymers with conducting properties opened up a new era in the field of polymer science. Over the last 17 years, conducting polymers (CPs) have attracted considerable interest because of their interesting electrical, electrochemical, optical and magnetic properties. Properties that lead to many uses, such as in corrosion inhibitors, compact capacitors, antistatic coating, electromagnetic shielding of computers, have been explored. A second generation of electric polymers has also appeared in applications like, *e.g.*, transistors, light-emitting diodes, lasers, television screens, solar cells, etc. Besides other promising applications such as electroluminescent

plastics films, sensors and biosensors, supercapacitors and batteries, drug delivery, artificial muscles, among others [7] [8].

Some of the most research and applied studies with CPs are related to polyheterocycles such as polythiophene (PTh), polypyrrole (PPy), poly(*p*-phenylene) (PPP), poly(*p*-phenylene vinylene) (PPV), poly(phenylene ethynylene) (PPE) and polyaniline (PAni) and their derivatives, because they exhibit good electrochemical and chemical stabilities, good conductivities and ease of synthesis. Their chemical structures are shown in Figure 1 [9].

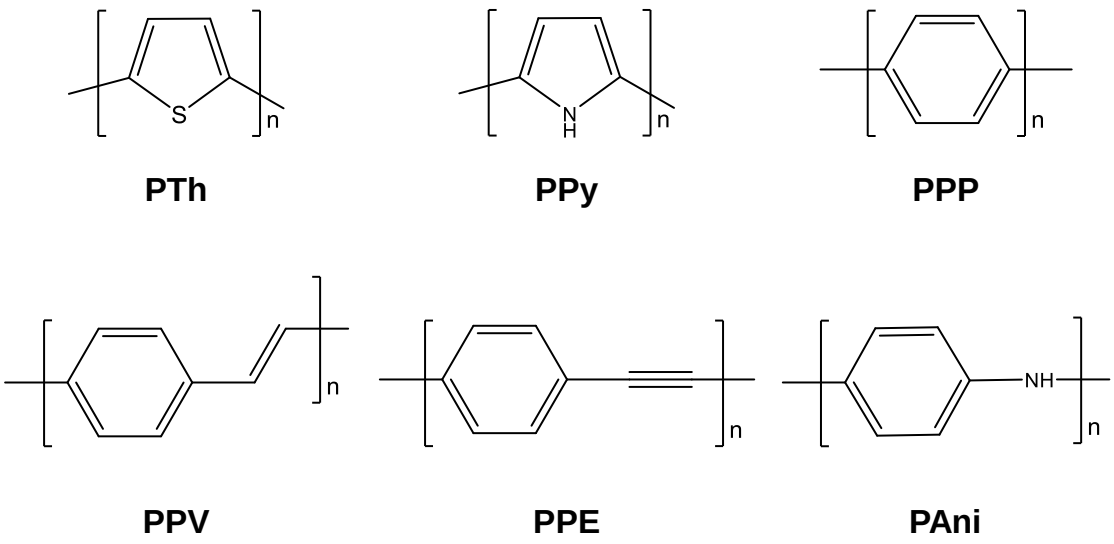

Figure 1: Chemical structures of semi-conducting polymers.

Polypyrrole (PPy) and its derivatives

As was mentioned, the PPy is one of the most frequently investigated polymers due to its great specific advantages such as relatively easy polymerization, low cost, environmental and thermal stability, high conductivity and charge storage capability.

Madden *et al.*, in 2004, studied different technologies which involve materials that change dimensions in response to an electrical input, one of them was PPy. They described its mechanisms as an electrochemically changing oxidation state that leads to the addition

or removal of charge from the polymer backbone and a flux of ions to balance charge, as depicted in Figure 2 [10].

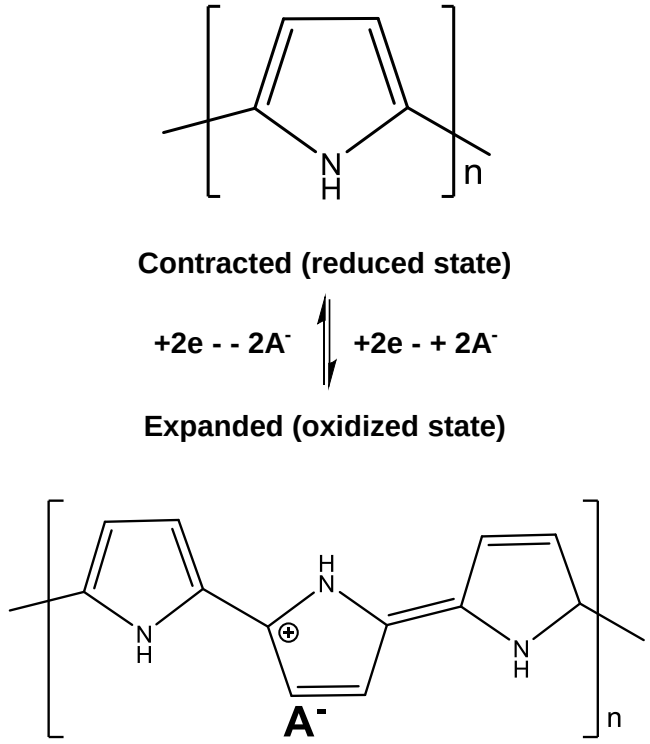

Figure 2: Polypyrrole response to dimensional changes, it expands as it is oxidized. Anions (A^-) enter to balance charge as electrons are removed. Expansion is generally correlated with net ion flux into the polymers.

Pyrrole derivatives also have captured the attention of various researches, the chemical structure of PPy was described in the Figure 1. However some of its derivatives are presented in the Figure 3.

In 2008, Alemán *et al*. [11] compared the formation of cross-links in PPy and poly(*N*-methypyrrole) (PNMPy), both polymers generated electrochemically. CV indicated that PNMPy was less electrostable than PPy but it was not due to electronic effects induced by the *N*-methylation even so, the tendency of polymer chains to grow regularly during the electropolymerization process was higher for PPy than PNMPy. It was attributed to the steric effects produced by the methyl group on PNMPy homopolymer. In 2012, the same

researchers synthesized compact films, solid microspheres with a porous internal structure, and core−shell microspheres with an ultrathin shell of poly(*N*-cyanoethylpyrrole) (PNCPy), by controlling polymerization method [12].

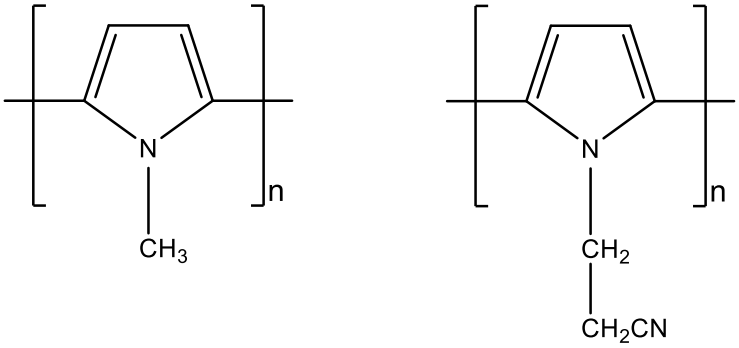

PNMPy **PNCPy**

Figure 3: Polypyrrole derivatives: poly(*N*-methypyrrole) (PNMPy) and poly(*N*-cyanoethylpyrrole) (PNCPy).

The modification of the form, structure and properties of CPs, like PPy, is essential to satisfy the specific requirements for different technological applications. A controlled method to modify these materials is the copolymerization, which results in copolymers with properties intermediate between the individual polymers. Thus, copolymerization allows obtain new materials with better and controlled properties overcoming the limitations usually associated to the preparation of new homopolymers. In recent years, copolymerization synthesis has been used to enhance the behavior of CPs as bioactive cellular matrices for engineering applications, modifying it with well-known biodegradable and biocompatible insulating polymers [13] [14].

1.2. Biocompatible polymers

In biomedical applications, there are continues efforts to enhance methods, materials and devices to allow improve the diagnostic and treatment of many diseases. Biocompatible polymer are a class of new generation of biomaterials that have demonstrated great

potential for biomedical devices, scaffolds for tissue engineering, drug delivery, biosensors and actuators [15]. Interactions between biocompatible polymer surfaces and organisms have been the focus of many studies, since the biocompatibility is one of the most important characteristics of a biomedical polymer whose surface interacts with a biological system.

Biocompatibility refers to the ability of a biomaterial to perform as an appropriate host in response of a specific situation, it means, ensures to be safe for use in the human body and in the endogenous fluids. To determine the biocompatibility of a given polymer, the protein adsorption on the material surface is usually evaluated, because it is believed to be the initial event when a material comes into contact with a biological environment. Therefore, the adsorbed protein layer will influence the subsequent biological reactions including platelet adhesion and activation [16] [17].

The most extensively used biocompatible polymers are poly(glycolic acid) (PGA), poly(lactic acid) (PLA) and their copolymers; polycaprolactone (PCL) and polyethylene glycol (PEG).

Poly(ethylene glycol) (PEG)

One of the most popular biocompatible materials used is poly(ethylene glycol) (PEG) also known as polyethylene oxide (PEO), which the chemical structure is shown in the Figure 4. This material can be used to restrict and control the attachment of cells and proteins on scaffolds since it is very hydrophilic. With the increase of hydrophilic properties, antibodies and other proteins are difficult to attach to the scaffolds, which allow a selective adsorption of specific proteins [18].

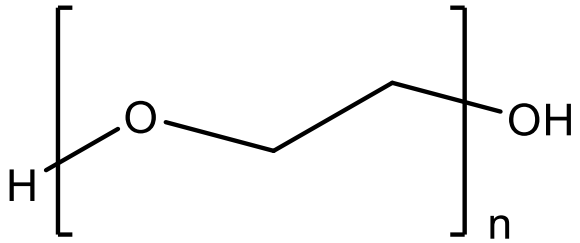

Figure 4: Poly(ethylene glycol) structure.

The major benefits of copolymerize monomers with different chemical structures is the high over the degree of control properties in the final material. Recently, several researchers have tried to copolymerize PEG with other non-biodegradable polymers in order to transfer its properties, such as, low toxicity, excellent solubility in aqueous solutions, extremely low immunogenicity, antigenicity, and others [19]. Therefore, the use of PEG in a copolymer is supposed to allow the control of the cell attachment and to enhance the biocompatibility of the copolymers. In 2013, Bendrea *et al.* [20] investigated the synthesis and electropolymerization of macromonomers combining polyheterocycles with insulating and biodegradable polymer, as PEG. They found that the hydrophilicity of the compounds increases with the PEG chains making the compounds excellent cellular matrices and suggesting multiple biotechnological applications, in which the transmission with cells is carried out at the electrochemical level.

This work is mainly focused on the copolymerization of PPy with a Schiff base macromonomer (compounds that contain the –C=N– functional linkage in their structure) formed by Py and PEG_{2000}, resulting in a new graft copolymer for possible applications as electroactive and biocompatible platforms. In the next chapters we will explain in detail the aim of the present work, the methodology employed for polymer synthesis and characterization, the results obtained, an estimated production costs and environmental impact, finishing with the proper conclusions.

2. Objectives

Electroactive biomaterials are a part of a new generation of ‘‘smart’’ biomaterials that can allow the direct delivery of electrical, electrochemical and electromechanical stimulators to cells. Within the family of electroactive biomaterials, conductive polymers enable excellent control of the electrical stimulus, possess very good electrical and optical properties, have a high conductivity/weight ratio and can be made biocompatible and biodegradable [21].

Based on the current importance of electroactive biomaterials, the present work proposes to copolymerize films from well-known EAPs, PPy, and a macromonomer synthesized from pyrrole backbone with chains of PEG_{2000} grafted. From electrochemical synthesis, it is intended to obtain a hydrophilic film with biocompatible and electrical properties that can contribute as promising bioactive platforms for engineering applications. The designed chemical structure of the graft polymer is shown in the Figure 5.

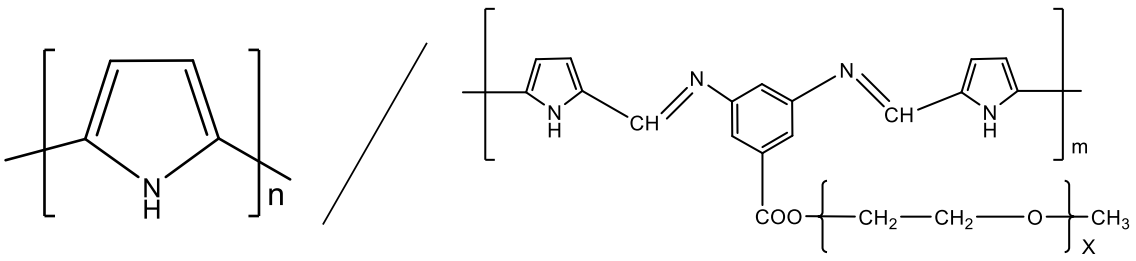

PPy **PAB53**

Figure 5: Graft copolymer of P(Py-*co*-PAB53).

Thus, the main aims of the present work are detailed below:

- Select and apply a synthetic methodology for obtaining a graft copolymer consisting in PPy units and a macromonomer with PEG_{2000} grafted (PAB53).
- Study the morphology and the wettability properties of the films obtained.
- Analyze the electroactivity, optical and conductive properties of the new copolymer.
- Examine the potential applications of the graft copolymer as active surfaces for selective adsorption of proteins.

3. Methodology

The aim of this investigation was polymerize, by electrochemical synthesis, a bioactive compound of Py-*co*-PAB53 and also evaluate its main properties. For this purpose, several techniques were employed. All the procedures, techniques and equipment used are explained below.

3.1. Materials

The macromonomer AzbPy-*g*-PEG was synthetized in the laboratories of Prof. Ian Cianga, from the Institute of Macromolecular Chemistry “Petru Poni” Iasi (Romania). The characterization of the macromonomer, that incorporates a polymeric chain of PEG, was performed by FTIR and H-RMN [see Annex A]. In this work the macromonomer AzbPy-*g*-PEG was simplified to PAB53.

Pyrrole monomer (Sigma-Aldrich, 98%) was distilled under reduced pressure before use, anhydrous lithium perchlorate (Sigma-Aldrich, 95%) was stored in an oven at 80°C before its use in the electrochemical trials and the solvent, acetonitrile (Panreac S.A., PA) was used as received. For the cellular adhesion, were used Bovine Serum Albumin (GIBC) and Lysozyme from chicken egg white (Sigma-Aldrich). During the characterization, the following reagents were used: Coomassie® (Merck) and TEMED (Amresco), Tris base, Sodium dodecyl sulfate, Basal Medium Eagle, Ninhydrin Reagent (2%), Acrylamide/Bis-acrylamide (30%) and Gel loading solution for electrophoresis; all provided by Sigma-Aldrich and used as received.

3.2. Copolymer synthesis

P(Py-*co*-PAB53) and PPy films were obtained by chronoamperometry in a VersaStat II potenciostate-galvanostate connected to a computer and controlled through a Power Suite Princeton Applied Research Program.

The polymerizations were carried out in a standard three electrode one compartment cell, showed in Figure 6, at room temperature. Using as working electrodes stainless steel

AISI 316L and ITO, with dimensions of 1.0 × 0.5 cm^2, the same metal alloy was used as counter-electrode and, as a reference, Ag|AgCl electrode containing KCl saturated aqueous solution (E° = 0.222 V at 25 °C). The cell was filled with solutions prepared in acetonitrile containing 0.1 M of $LiClO_4$, as dopant agent, and 1mM of Py or Py:PAB53 (molar ratio 1:1), as monomers. For the preparation of PPy films, it was necessary apply a constant potential of +1.7 V during a polymerization time of θ = 300 seconds. On the other hand, the applied potential for P(Py-*co*-PAB53) films was +1.6 V during θ = 300, 500 and 1000 seconds. Each potential was determined by anodic polymerization of the corresponding solution, which were studied by cyclic voltammetry (CV).

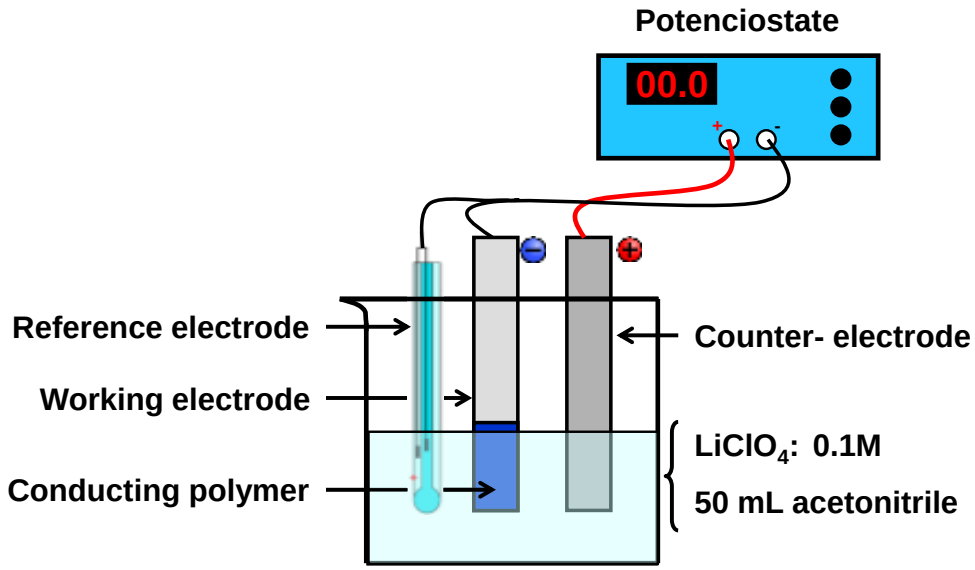

Figure 6: Scheme of a three electrode one compartment cell.

3.3. Physical-chemical characterization

3.3.1. Fourier Transform Infra-red Spectroscopy (FTIR)

FTIR is a sensitive technique applied in analytical chemistry for the characterization of molecules, it has proved to be useful and a popular tool in identification and characterization of organic materials. It is based on the fact that molecules absorb specific frequencies that are characteristic of their structure; these absorptions are related to the strength of the bond [22].

For this work, the FT-IR spectra of monomers and electropolymerized polymers were recorded on a Nicolet 6700 spectrophotometer equipped with a transmission accessory and using KBr pellets. The samples were evaluated using OMNIC software at 64 scans between 4000 and 600 cm^{-1} and resolution of 2 cm^{-1}.

3.3.2. Scanning electron microscopy (SEM)

The scanning electron microscope is a powerful instrument which permits the observation and characterization of heterogeneous organic and inorganic materials and surfaces on a specific scale. The area to be examined is irradiated with a finely focused electron beam, producing secondary and backscattered electrons signals that can be used to examine many characteristics of the sample (composition, surface topography, crystallography, and others) [23].

The morphology of the prepared films was examined by SEM using a Focused Ion Beam Zeiss Neon40 scanning electron microscope operating at 5 kV.

3.3.3. Atomic Force Microscopy (AFM)

AFM is a local probe technique that can be used as an imaging instrument, a force sensor and actuator and as a molecular sensor. For this investigation it allows to obtain topographic images of the films surface, obtained with an AFM Dimension microscope using a NanoScope IV controller under ambient conditions in tapping mode [24].

The row scanning frequency was set between 0.7 and 0.9 Hz, the scan window size was 5 x 5 μm^2 and the Root Mean Square roughness (RMS Rq), which is the average height deviation taken from the mean data plane, was determined using the statistical application of the NanoScope Analysis software (7.30, Veeco).

3.3.4. Optical profilometry

The thickness of the films was determined using a surface profilometer Dektak 150 (Veeco). Intentionally, only partial area of the electrode was left to polymerize, the other was covered with an adhesive tape in order to obtain a step for the thickness measurements. Therefore, the resulting step was measured in several parallel lines by the computer software Dektatk (version 9.2, Veeco Instruments Inc.) to allow statistical analysis of data. In

the Figure 7, it can be see the difference between the electropolymerized film and the uncovered metal substrate for the three polymerization times.

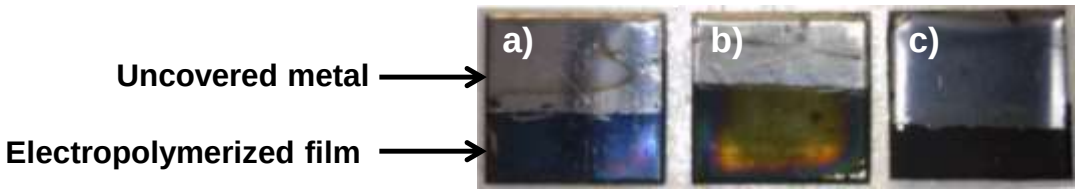

Figure 7: Scratch throughout the surface of the P(Py-*co*-PAB53) generated at a) 300s, b)500s and c)1000s.

3.3.5. Water contact angle (WCA)

When a gas and liquid, separated by their common interface, come in contact with a solid surface, the contact line between the three phases is called the common line (CL) and the contact angle (θ) is the one between the liquid–solid and liquid–gas interfaces, Figure 8. If θ is lower than 90°, the surface is called hydrophilic, whereas if θ is greater than 90°, the liquid is non-wetting, so the surface is called hydrophobic [25].

The hydrophobicity of the samples were recorded and analyzed at room temperature on a contact angle measuring device OCA-15EC from DataPhysics Instruments GmbH. Using a metallic needle (Hamilton 100 µL) 1 µL of distilled water was dropped on the horizontal surface of each film, in a drop contour digital image the common line (CL) was draw and the θ between the CL and the drop was measured by the software SCA20 (DataPhysics Instruments GmbH).

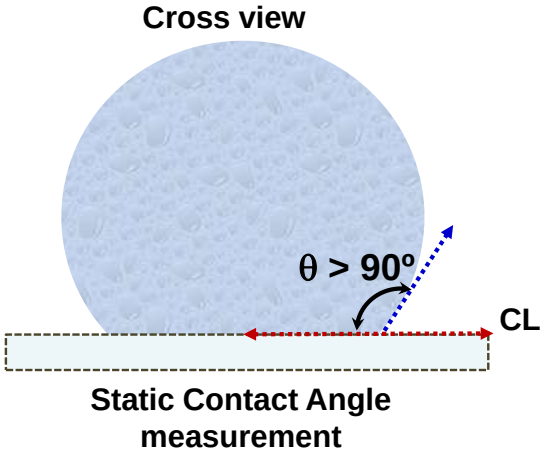

Figure 8: Water contact angle at the liquid–gas–solid interfaces.

3.3.6. Electrochemical properties

Cyclic voltammetry (CV) is a versatile electroanalytical technique for the study of electroactive species, it allows rapidly observe the redox behavior over a wide potential range. CV is obtained by measuring the current at the working electrode during the potential scan; this current can be considered the “response signal” to the potential excitation signal.

Using Autolab PGSTAT302N equipped, it was possible determined the electroactivity (charge storage ability) and the electrostability (loss of electroactivity with consecutive oxidation-reduction cycles) of the films in this study.

The assay was carried out in a standard three electrode cell similar to the electropolymerization procedure, the solvent used was acetonitrile containing 0.1 M of $LiClO_4$ in a potential range from -0.5 to 2 V, 50 mV/s as scan rate and 49 consecutive oxidation-reduction cycles. The electrostability (LEA, %) was evaluated by the Equation 1, where ΔQ is the difference between the oxidation charge (C) of the second and the last cycle, and Q_I is the oxidation charge corresponding to the first cycle.

$$\%LEA = \frac{\Delta Q}{Q_I} * 100 \qquad \text{Eq. (1)}$$

3.3.7. Ultraviolet–visible spectroscopy (UV-Vis)

It refers to absorption spectroscopy or reflectance spectroscopy in the ultraviolet-visible spectral region, is used primarily to study organic compounds that absorb radiation in patterns that can reveal information about the molecules structure [26].

In this investigation, the spectra were obtained using a UV-vis-NIR Shimadzu 3600 spectrophotometer equipped with a tungsten halogen visible source, a deuterium arc UV source, a photomultiplier tube UV-vis detector, and a InGaAs photodiode and cooled PbS photocell NIR detectors. PPy and P(Py-*co*-PAB53) films were deposited onto ITO and were evaluated between 300 nm and 800 nm, in the absorbance mode using the integrating sphere accessory (model ISR-3100). In the assembly shown in Figure 9, two holders of the integrating sphere are coated with highly diffuse $BaSO_4$ reflectance standard, whereas the other two positions are reserved for the reference and polymer film samples.

Measurements, data collection and data evaluation were controlled by the computer software UVProbe version 2.31.

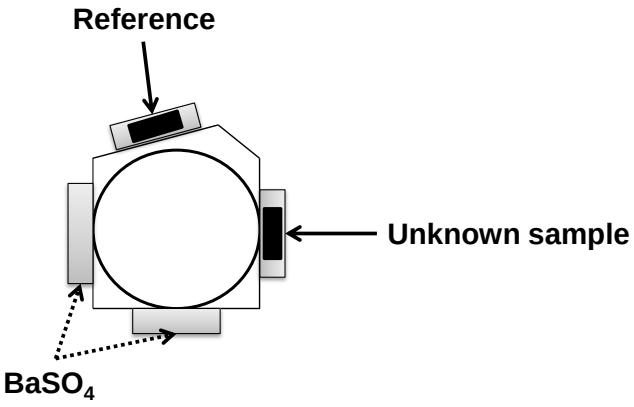

Figure 9: Transmittance measurement of solid samples.

3.3.8. Cellular adhesion

In order to investigate the ability of the P(Py-*co*-PAB53) 1000s films to interact with different types of proteins, adsorption protein assay was carried out using albumin (BSA) and Lysozyme (Lyz) both globular proteins. More information can be found in the Annex B.

P(PAB53-*co*-Py), PPy and steel substrates were immersed in 500 µL of BSA and Lyz solutions, both al 1% in water, during 48 hours at 37 °C with moderate stir. After time, the samples were washed with deionized water and dried at room conditions. Once every electrode were completely dry, 300 µL of extraction buffer (Tris 0.625M, SDS 2%, BME 5%) were added and incubated for one hour.

Protein concentration by Ninhydrin reaction

Ninhydrin reactions, using manual and automated techniques, are widely used to analyze and characterize amino acids, peptides, proteins and other Ninhydrin-positive compounds by photometric and colorimetric method. The reaction mechanism of the Ninhydrin hydrate with amino groups, produced the colored Ninhydrin chromophore called Ruhemann's purple (RP) ($A_{\lambda max}$ 570 nm), that can be explained by polar and steric effects associated with the reactants [27].

The protein concentration was calculated using Ninhydrin reactions evaluated by a colorimetric method. The solutions were prepared mixing the same amount of the proteins, extracted for the different surfaces, and Ninhydrin. Later the samples were heated at 95 °C for 10 min and the absorbance at 570 nm was measured in a microplate reader, EZ Read 400– Biochrom with ADAP 2.0 Plus Data Analysis Software. In order to get the concentration adsorbed, it was necessary to make a reference graph of different protein concentration *versus* the absorbance. The procedure was the same than for polymer samples but the proteins extracted were replaced for different known concentrations of Lyz and BSA solutions.

Electrophoresis

A relatively simple, rapid, and highly sensitive tool to study the properties of proteins, is based on the fact that charged molecules will migrate through a matrix upon application of an electric field, usually provided by immersed electrodes. Generally the sample is run in a support matrix such as agarose or polyacrylamide gel. The last one can be used to analyze the size, amount, purity, and isoelectric point of polypeptides and proteins [28].

Polyacrylamide gel used in this work was prepared at 12% resolving and 6% stacking, lyophilized samples were prepared adding gel loading buffer, as a tracking dye, to the extracted proteins in a relation 1:6 v/v of buffer and protein. Reference bands were loaded of BSA and Lyz solutions with the same tracking dye. All the samples were exposed to an electric field of 90 V for 2 h. Further, using a solution of Coomassie®–methanol-acetic acid (0.1%-40%-10%), the gel was colored and, later, washed-out with a solution of 40% of methanol and 10% of acetic acid.

4. Results and discussion

The P(Py-*co*-PAB53) films, obtained by electropolymerization, were evaluated analyzing their changes compared with PPy homopolymer, both synthetized by the same method of polymerization: chronoamperometry (CA). Some discussion related to the synthesis, characterization and biocompatibility property are presented below.

4.1. Electrochemical synthesis

Even though a number of different experimental conditions were tested for the electropolymerization of PAB53 homopolymer (*i.e.* electrolyte nature, electrode materials and/or different potential applied), no visible polymer was obtained. This PAB53 behavior could be explained due to the appearance of conjugated short chain-like structures, which prevent the electrochemical polymerization at high oxidation potential. Thus, radicals derived from monomers undergo rapid reactions with the solvent or anions to form soluble products rather than to electropolymerize [29].

With the aim to generate the necessary samples for this study, the electropolymerization of Py and PAB53 was carried out using chronoamperometry (CA). Previously a CV of the electrolyte solutions (pyrrole, PAB53 and the Py:PAB53) were carried out in order to stablish the better oxidation potential to generate the polymers. Therefore, using the resulting voltammograms, the potential applied during the CA was obtained as is shown in Figure 10 (dashed line). The optimum potential achieved was +1.7 V, +1.75 V and +1.6 V for pyrrole, PAB53 and Py:PAB53 monomers; respectively.

Regarding the polymerization process, the Figure 11 presents a typical curve obtained as a result of CA, on it the current intensity (I) is plotted versus the polymerization time. In all cases, after holding the current for 2s the monomers started to polymerize. The current intensity stabilizes after 60 seconds, indicating that the polymer was growing as well as doping, resulting in a semi-conducting polymer. The polymerization of pure macromonomer PAB53 failed in the present conditions, as explained before. The current intensity was almost 0.0 A. The better current intensity was found for the simplest Py monomer (9.56 E-4 A) due to the ease and fast mobility of pyrrole molecules from the electrolyte solution.

Despite the low concentration of both monomers, Py and PAB53, on the electrolyte solution (1 mM), it was possible to obtain a copolymer film in only 5 minutes of electrochemical charge. Increase of polymerization time results in increased film thickness, as was observed by profilometry.

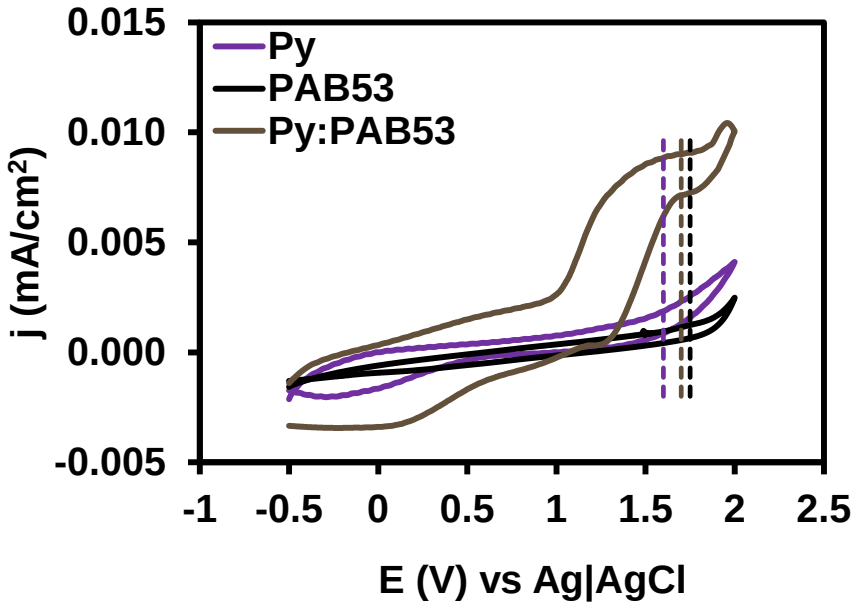

Figure 10: Cyclic voltammograms of the electrolyte solution of pyrrole, PAB53 and Py:PAB53 (50:50) measured from -0.5 to 2 V.

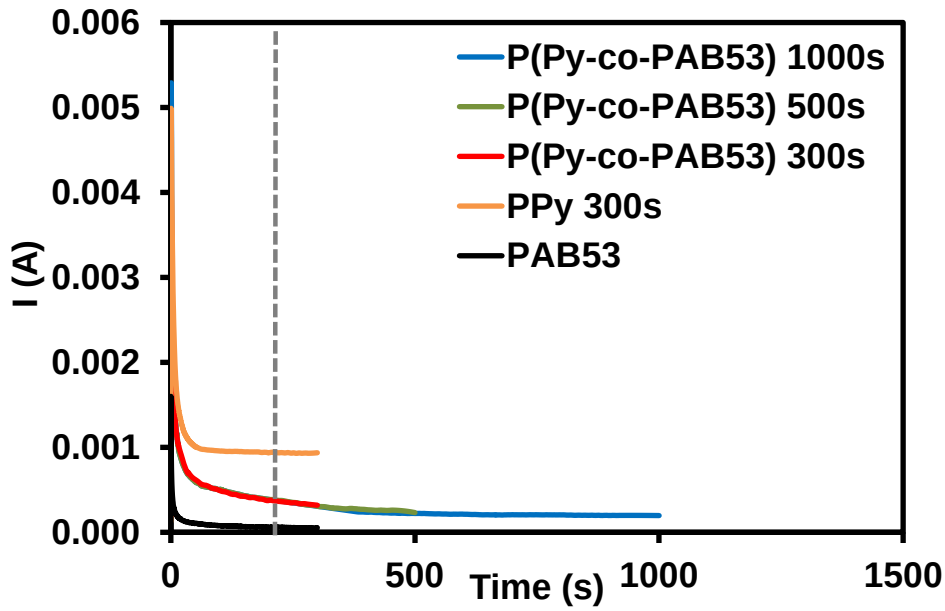

Figure 11: Synthesis of the films by chronoamperometry at +1.7 V, +1.75 V and +1.6 V for pyrrole, PAB53 and the copolymers P(Py-*co*-PAB53).

ETSEIB

4.2. FTIR spectroscopy of P(Py-*co*-PAB53) films

The FTIR spectra of monomers (Py and PAB53), homopolymer (PPy) and copolymers P(Py-*co*-PAB53) generated at 300, 500 and 1000s are included in Figures 12 and 13.

In the Figure 12, we can appreciate a comparison between the pyrrole monomer and the resulting homopolymer. One of the main characteristic of the infrared from polymers is their broad and less intense absorption bands compared to the monomer. The absorption bands in Py monomer are very sharp and well-defined, which main peaks correspond to: N-H stretching vibration, C-H$^{\alpha}$ and C-H$^{\beta}$ stretching and bending vibrations, C=N, C=C and C-N stretching vibrations; and C-H and N-H deformations. The main absorption bands for all systems are resumed in the Table 1.

Detail inspection of FTIR spectra leads to the conclusion that the homopolymer was well obtained from electropolymerization. The absorbance due to the aromatic C-H stretch at ~3102 cm^{-1} can be attributed to the β-hydrogen whereas the band at ~3125 cm^{-1} is related to the α-hydrogen position in the pyrrole ring. Additionally, the β C-H out-of-plane deformation is usually observed as a medium peak at 864 cm^{-1} while the α C-H out-of-plane deformation appears as a very sharp band at 720 cm^{-1}. As we can be seen in the FTIR spectrum of PPy, the strong peak at about 720 cm^{-1} related to the α C-H out-of-plane deformation disappears indicating that the α positions (2,5 positions, alternatively) of pyrrole units have been successfully attached. The other absorption bands in PPy films are similar to the starting monomer. The first one corresponds to N–H stretching vibrations (3000-3668 cm^{-1}), C=N Schiff base vibrations (1727 and 1628 cm^{-1}), C=C stretching of pyrrole ring (1526 cm^{-1}), bands from C-H in-plane vibration (1146, 1114 and 1082 cm^{-1}) and C-H out-of-plane (888, 776 and 627cm^{-1}) [30] [31] [32] [33].

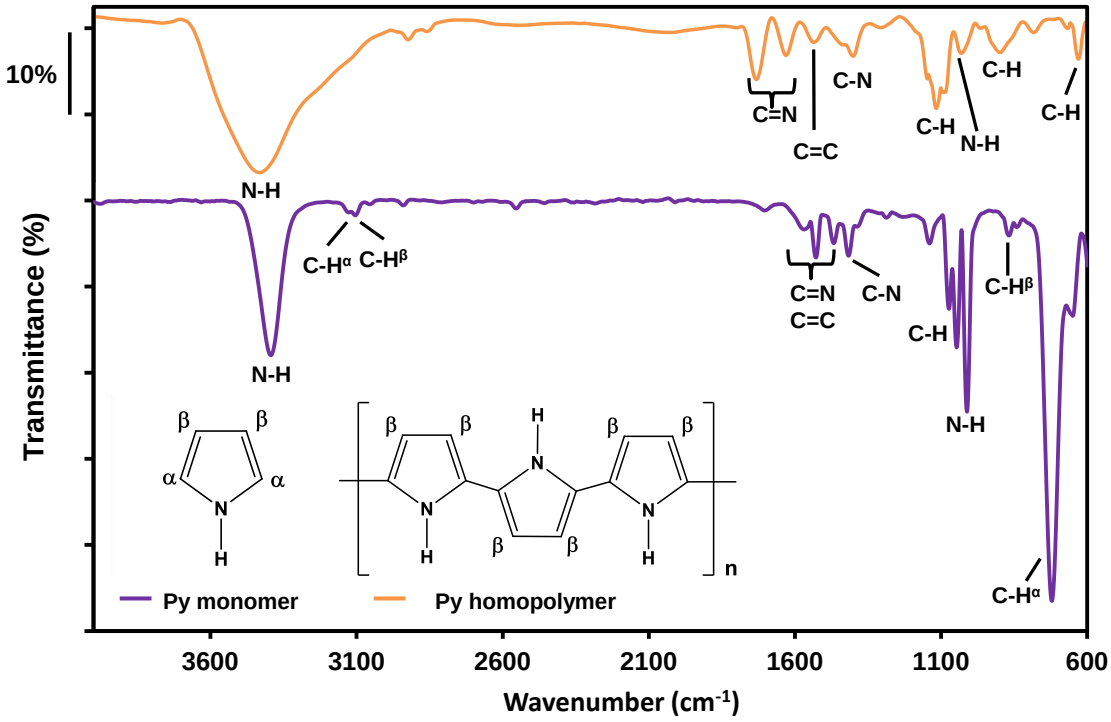

Figure 12: Infrared spectra of pyrrole (Py) and polypyrrole (PPy) molecules.

The monomer of pyrrole grafted with PEG chains was also characterized by FTIR. PAB53 spectrum exhibited less absorption bands of pyrrole units due to the great contribution of PEG bands, *i.e.* due to its long –[O-CH_2-CH_2-]- chain. Therefore, from pyrrole ring only three main peaks are localized: N–H stretching vibrations (3140-3648 cm^{-1}), C=C stretching of pyrrole ring (1625 cm^{-1}, together with benzene group), and C-N stretching vibration (1347 cm^{-1}). On the other hand, from PEG units several sharp bands, like methylene C–H symmetric stretching band at 2885 cm^{-1} and at 1470 cm^{-1}, typical from CH_2 scissoring vibrations were clearly visible. The band at 1347 cm^{-1} was also derived from CH_2 wagging of PEG, whereas strong bands from (C=O) ester (C–O-C) and ether group appeared at 1716 cm^{-1}, 1281 cm^{-1}, 1239 cm^{-1} and 1110 cm^{-1} (Figure 13) [34]

As was explained before, the electrochemical synthesis of PAB53 homopolymer turned out in no polymer obtained. Therefore, the characterization was only perfomed for copolymers between pyrrole and PAB53 monomers. In the Figure 13, the absorption bands of the copolymers generated with three CA times are shown. All them show characteristics peaks of PPy and PAB53 confirming that the films studied were generated correctly.

However, it is noteworthy that the copolymer generated at 1000s had greater contribution from PAB53 monomer than pyrrole, with the same molar ratio (50:50). With small polymerization time, less PAB53 is able to reach the metal substrate and copolymerize. It is probably due to a saturation on the electrode of Py monomers, with highest mobility than PAB53 monomer (interface metal-polymer). The main absorption bands of P(Py-*co*-PAB53) generated at 1000s are summarized in the Table 1.

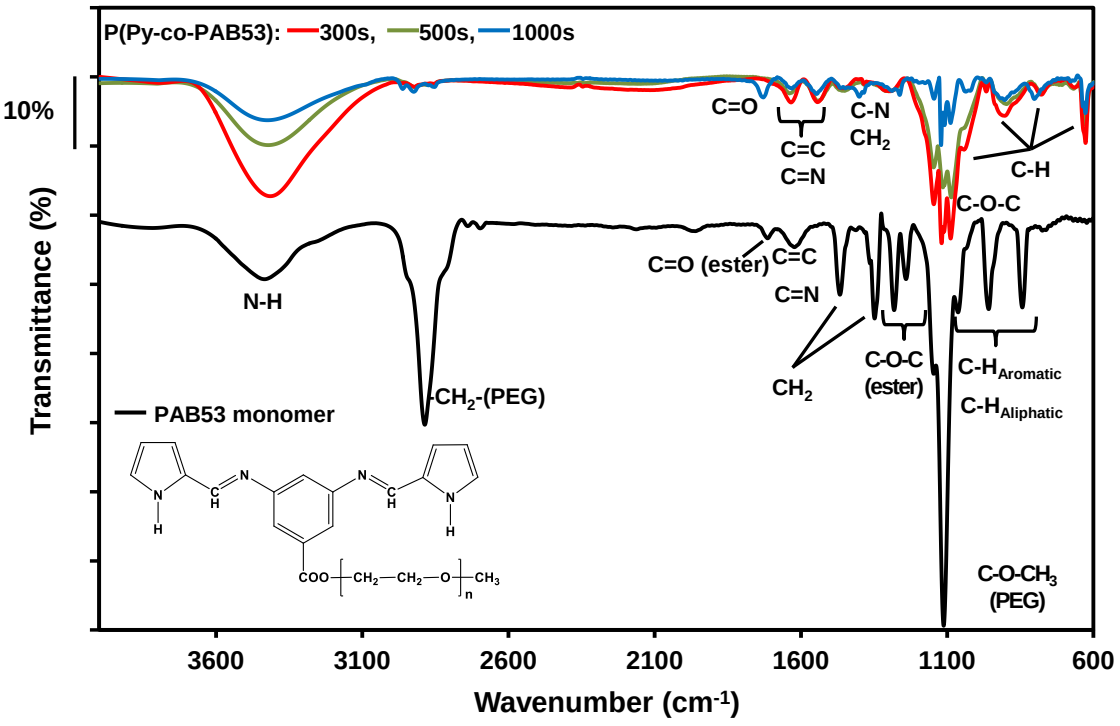

Figure 13: Infrared spectra of Py-PEG-grafted monomer (PAB53) and copolymer [P(Py-*co*-PAB53)].

Table 1: FT-IR assignments for the main vibrations of PPy and PAB53.

Vibrational wavenumbers (cm^{-1})				Assignments
Py	PPy	PAB53		
		Py	*PEG_{2000}*	
3391				N-H stretching vibrations
3125				C-H^{α} stretch (pyrrole ring)
3102				C-H^{β} stretch (pyrrole ring)
864				C-H^{β} out-of-plane deformation
720				C-H^{α} out-of-plane deformation
	3431			N-H stretching vibrations
	1628			C=N Schiff base vibrations
	1526			C=C stretching of pyrrole ring
	1429			C-N stretching
	1396			C-N stretching
	1146			C-H in-plane vibration
	1114			C-H in-plane vibration
	1082			C-H in-plane vibration
	1021			N-H in plan deformation
	888			C-H out-of-plane deformation
	776			C-H out-of-plane ring deformation
	627			C-C out-of-plane ring deformation or C-H rocking
		3140-3648		N-H stretching vibrations
		1625		C=C stretching of pyrrole ring / Benzene group
		1347		C-N stretching vibration
			2885	C-H symmetric stretching
			1716	C=O group from ester linkage
			1470	C-H_2 scissoring vibrations
			1281	C-O-C ether group
			1239	C-O-C ether group
			1110	C-O-C ether group

4.3. Morphology, topography and thickness evaluation

The morphology of the copolymers formed by the macromonomer PAB53 and Py at different polymerization times were studied using SEM technique. Micrographs at low magnification demonstrated that polymerization time was an important factor to take into account to generate polymer films because it will influence the electrochemical stability of the conducting polymers as a result of increased crosslinking between chains [11] [35].

Figure 14a revealed that the metal bare (indicated by arrows) was not completely covered by the conducting polymer film with 300s of polymerization. Close inspection from the zones with polymer adhered (Figure 14b) revealed that the morphology is similar to PPy homopolymer, *i.e.* cauliflower-like structures [36] [31]. It led us to conclude that the content of PAB53 in P(PPy-*co*-PAB53) copolymer is extremely low with t_{pol}= 300s.

On the other hand, Figures 14 (c-f) showed that with longer polymerization time the metal substrate is completely covered and cauliflower-like aggregates increased. However, the presence of PAB53 does not change substantially the surface morphology. As can be observed in the same Figure 14f, when the concentration of PAB53 monomer in the copolymer films increased, the presence of PEG chains seems to favor the formation of valleys and hills and also decrease the presence of agglomerates. It should be highlighted that in any case none phase separations or cracks were observed.

As was demonstrated, polymerization time was a parameter that influenced in the amount of adhered polymer onto the surface and roughness film, the last one was studied by AFM. The analysis was performed with PPy homopolymer and the copolymers generated at 300, 500 and 1000s.

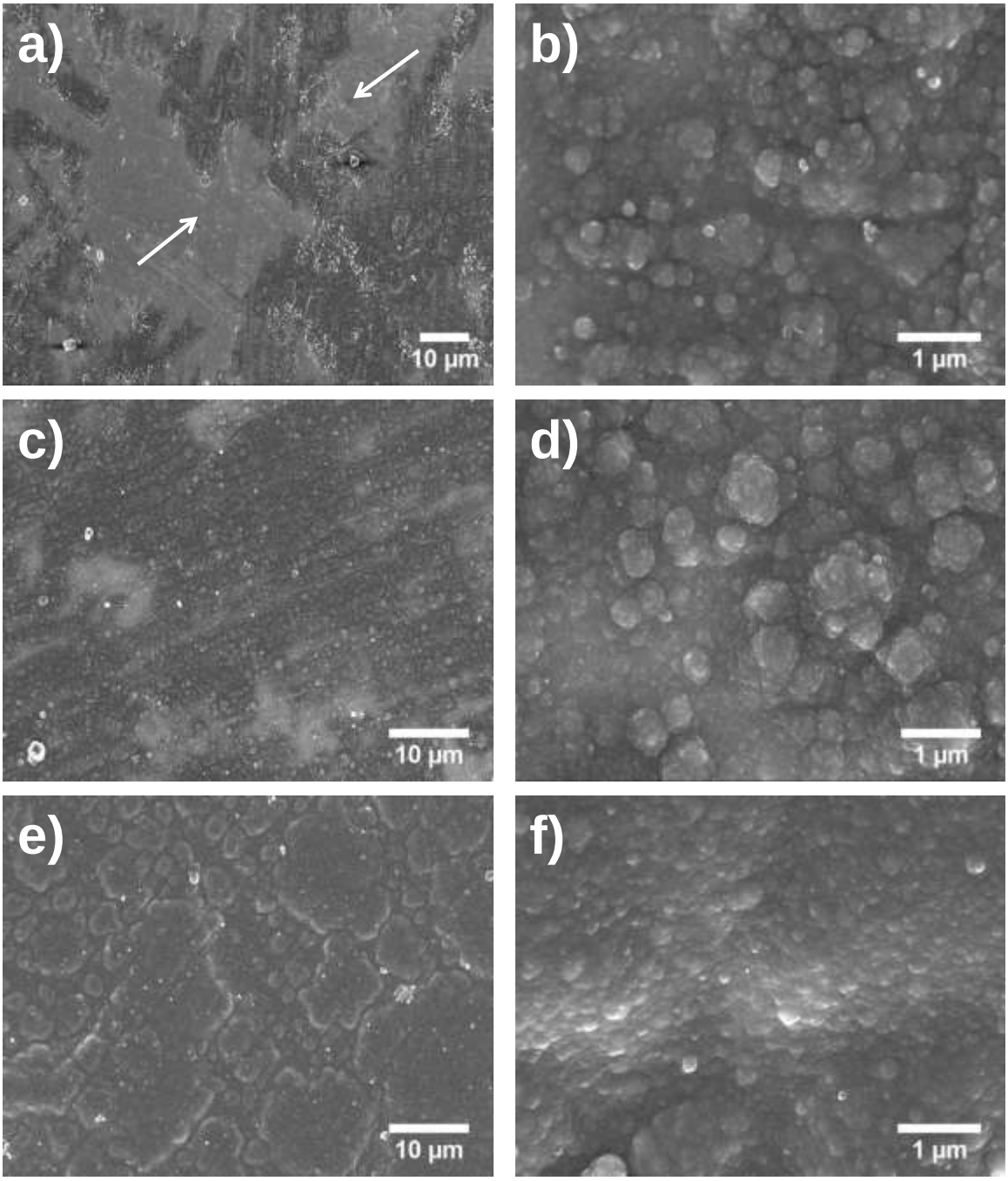

Figure 14: SEM Micrographs of P(Py-*co*-PAB53) at polymerization time of 300s (a, b), 500s (c,d) and 1000s (e,f).

Comparing 2D Height and 3D topographic AFM images between PPy and P(Py-*co*-PAB53) with 300s of polymerization time (Figure 15 a and b). It was observed a remarkable difference of coated area, attributed to the length of the chain grafted (PEG_{2000}) into the macromonomer, which hinders a uniform polymerization. A similar effect was detected to P(Py-*co*-PAB53) generated at 500s but the coated area increases at 1000s of electropolymerization. In order to confirm these observations, the roughness of the materials was measured with two different scan areas. In the first one, the roughness was measured in an area of 5 x 5 μm^2 (A), it might not be very precise because it would take into account areas without adhered polymer. The second one, which was more accurate than the first; measuring areas of 2 x 2 μm^2 (B) allows calculate the roughness in areas completely covered by polymer film.

The roughness obtained with A and B measurements are presented in Table 2. Both analyses follow a similar tendency, high polymerization time implies more roughness and, consequently, high amounts of adhered polymer (high thickness, Table 3).

Considering that P(Py-*co*-PAB53) 1000s had biggest coated zones, it could be expect that the roughness is more homogenous for this film than the other two, as was evidenced by the lowest deviation value obtained in 2 x 2 μm^2 of scan area.

With respect to the thickness, as it was previously commented, the polymer films with the highest thickness were the one generated at 1000s. Additionally, the thickness between P(PAB53-*co*-Py) 1000s and PPy was almost twice (Table 3). This confirmed the theory that on the copolymer surface, PEG chains could be the molecules responsible for the valleys and hills observed in SEM images. Also it explained why, even if P(PAB53-*co*-Py) 500s had less amount of material, its roughness and thickness was similar to the homopolymer obtained with 300s.

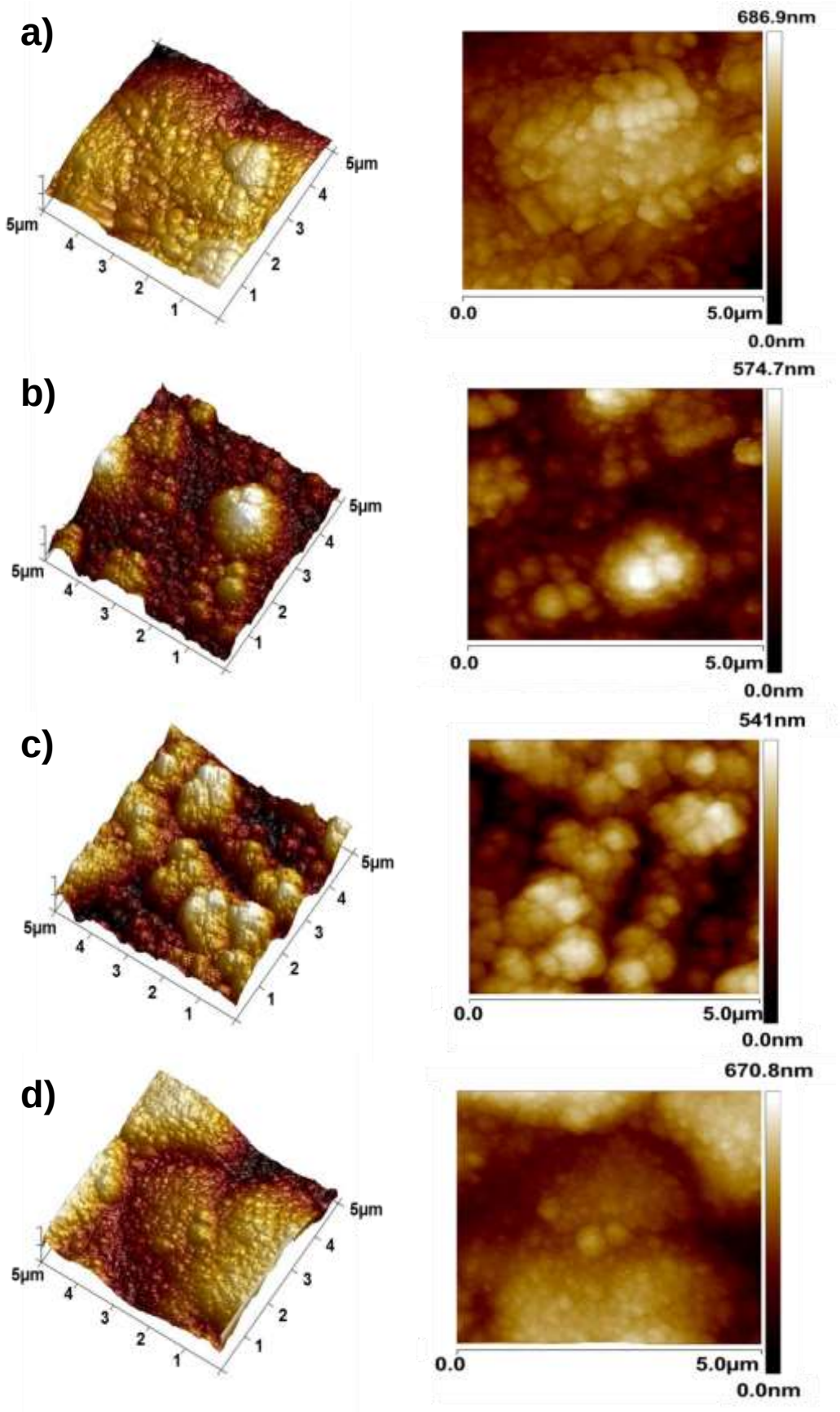

Figure 15: 2D Height and 3D topographic AFM images of a) PPy 300s and the copolymer films at b) 300s, c) 500s and d) 1000s.

Table 2: Roughness of PPy and P(Py-co-PAB53) films, measured by AFM, and employing areas of 5 x 5 μm^2 (A) and 2 x 2 μm^2 (B).

Sample	Roughness A (nm)	Roughness B (nm)
PPy 300s	**112**	**76 ± 1.2**
P(Py-*co*-PAB53) 300s	**91**	**58 ± 1.8**
P(Py-*co*-PAB53) 500s	**102**	**68 ± 1.5**
P(Py-*co*-PAB53) 1000s	**123**	**82 ± 0.6**

Table 3: Thickness average of PPy and P(Py-co-PAB53) films obtained by profilometry.

Sample	Thickness average (µm) ± deviation
PPy 300s	**2.2 ± 0.1**
P(Py-*co*-PAB53) 300s	**1.4 ± 0.4**
P(Py-*co*-PAB53) 500s	**2.6 ± 0.5**
P(Py-*co*-PAB53) 1000s	**4.1 ± 0.5**

4.4. Wettability

It has been reported that the wettability of surfaces is governed by three main parameters: the liquid-repellent properties of the compounds present at the surface, the surface morphology or topography and also the roughness [37].

The relationship between roughness and wettability was defined in 1936 by Wenzel who indicated that adding surface roughness will enhance the wettability caused by the chemistry of the surface, based on the assumption that the liquid penetrates into the roughness grooves, as in Figure 16. So if the surface is chemically hydrophobic, it will become even more hydrophobic when surface roughness is added [38].In the field of polymeric materials, it has been studied how different polymerization techniques can control the surface morphology and the roughness geometry at micro- or at nanoscale with a surface wettability going from superhydrophilicity to superoleophobicity [37].

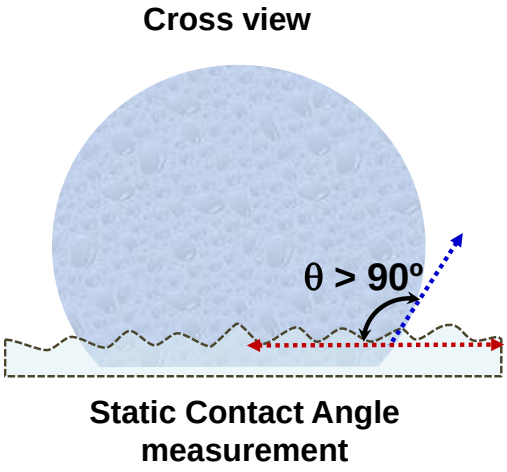

Figure 16: Water contact angle on rough surface, Wenzel model.

As was expected all studied films were hydrophilic displaying water contact angles (θ) lower than 90° due to the presence of the polar groups from pyrrole rings (N-H) and pyrrole ramification (PEG chain). PEG is well known by its hydrophilic properties in water and also high solubility in water, alcohols, dichloromethane, acetonitrile and other polar solvents. Nevertheless, in the present study the wettability observed can be explained in basis on the

roughness of films, which increase with the presence of PEG chains favoring the formation of valleys and hills, as was previously observed by SEM.

Thus, it is clear that the incorporation of the PEG chains in pyrrole rings improves the liquid-absorption properties onto polymer surfaces, corroborating our initial hypothesis that PEG will appear as outer layer, after the first pyrroles units adhered to the metal bare, *i.e.* as inner interface. Hence and in congruence with previous results, the most hydrophilic film was the one generated at 1000s improving the film wettability almost twice.

The average values of the water contact angle (θ) determined for PPy, P(Py-*co*-PAB53) at different polymerization times and steel (reference) are show in the Table 4.

Table 4: Values of water contact angle (θ, in degrees).

Sample	θ (°)
Steel	**88.3 ± 0.1**
PPy 300s	**58.9 ± 0.1**
P(Py-*co*-PAB53) 300s	**71.0 ± 0.4**
P(Py-*co*-PAB53) 500s	**62.6 ± 0.3**
P(Py-*co*-PAB53) 1000s	**48.5 ± 0.3**

4.5. Electrochemical stability of P(Py-*co*-PAB53) copolymer

The amount of exchanged charge during the first cycle (electroactivity) was determined evaluating the oxidation and reduction cycles in the corresponding voltammograms. As can be seen in Figures 17a and b, the electroactivity decreased almost 0.034 C in the films containing PEG, compared to PPy homopolymer, both generated at 300s. Therefore, the length of the chain grafted to aromatic unit hindered the optimum charge mobility across the copolymer chains causing a negative effect on the electrochemical stability and, consequently, on the electrical conductivity. On the other hand, the incorporation of PEG chains do not decrease abruptly their ability to store charge after 50 cycles, as is evidenced by the % of LEA (Table 5). This information permitted us to reaffirm that with a shorter polymerization time less copolymer was obtained onto the metal substrate and therefore less amount of PEG was incorporated to the copolymer film.

Table 5: Electroactivity and electroestability of the films obtained.

Sample	Electroactivity (C)	Electrostability (%LEA)
PPy 300s	0.052	48.32
P(Py-*co*-PAB53) 300s	0.018	19.11
P(Py-*co*-PAB53) 500s	0.021	29.91
P(Py-*co*-PAB53) 1000s	0.024	37.66

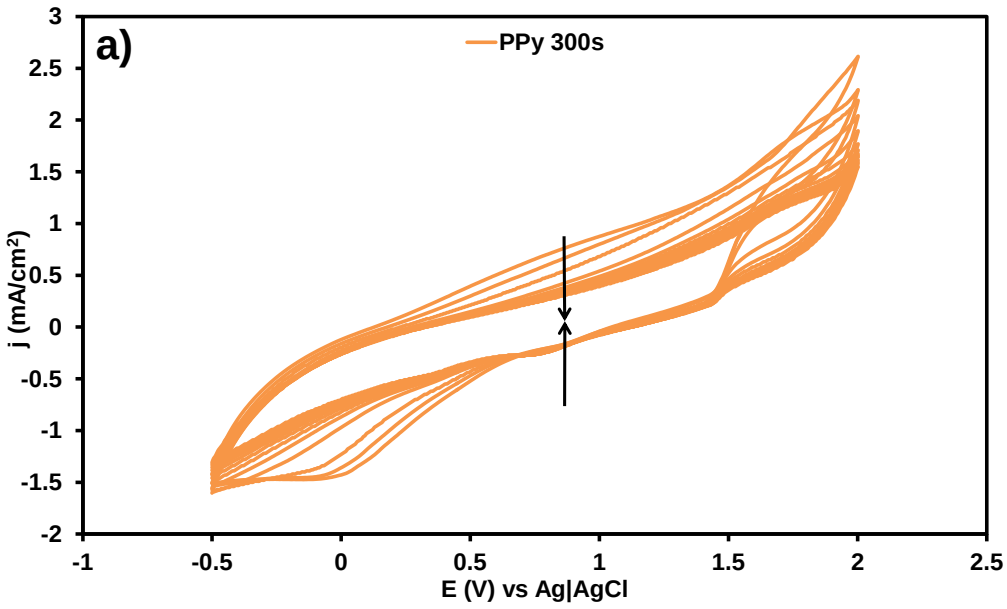

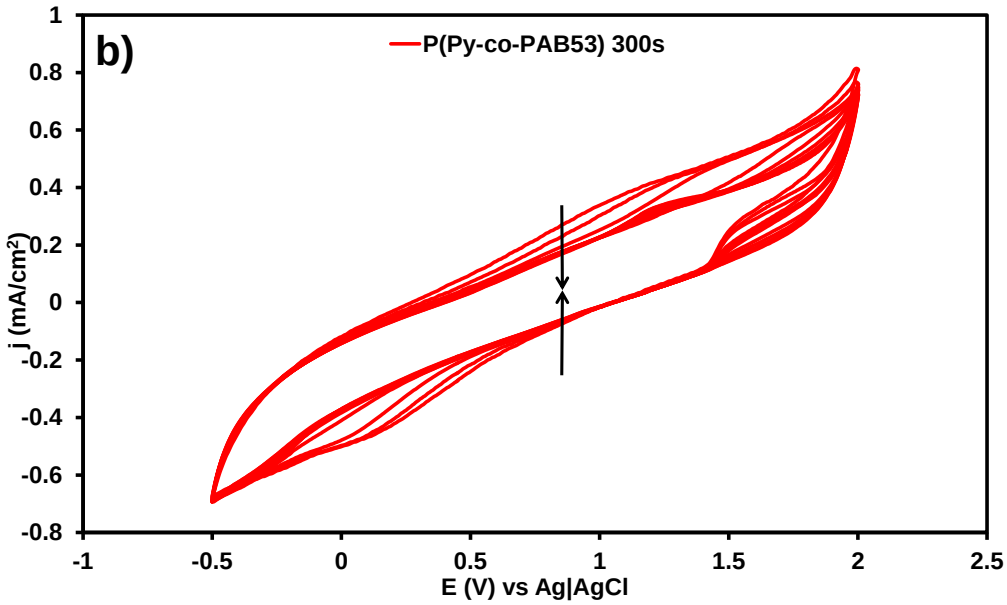

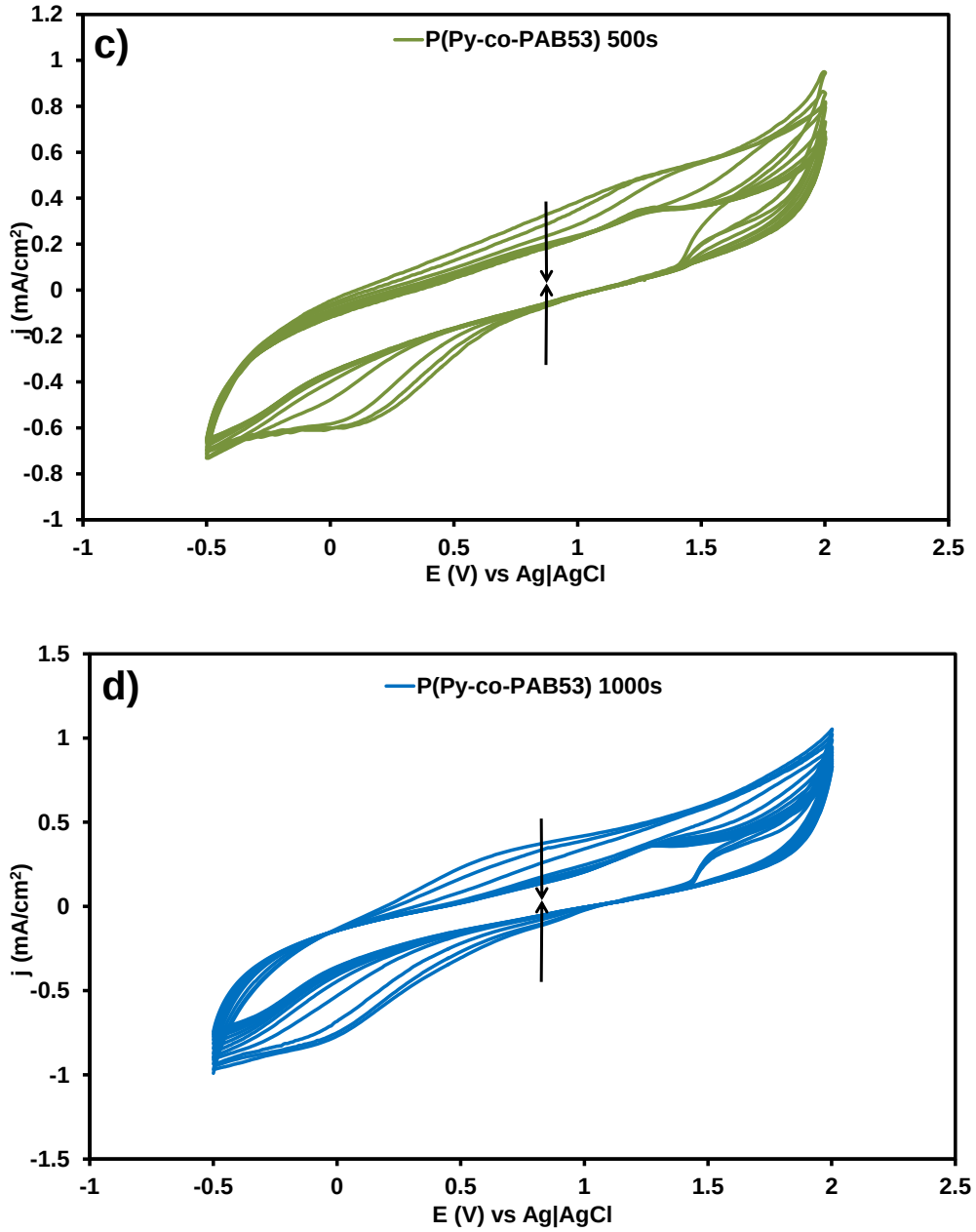

Figure 17: Cyclic voltammograms of a) PPy homopolymer (300s) and copolymers generated at b) 300s, c) 500s and d) 1000s. The arrows indicate the direction from cycles one to fifty.

4.6. Optical and conductive properties

The UV–vis absorption spectra of PPy and P(Py-*co*-PAB53) generated at 300s, 500 and 1000s are shown in the Figure 18. All the films exhibited a characteristic absorbance peak at 445 and 448 nm (homopolymer and copolymers), which is associated with π–π* electron transition of conjugated PPy rings [39]. The shoulders around 322 - 346 nm can be attributed to the presence of short oligomers that still reside inside the film [40]. It should be highlighted that at less polymerization time, less well-defined absorption bands. It could be due to the ITO surfaces with not homogenously covered P(Py-*co*-PAB53) films. Thus, it may cause that UV−vis spectroscopy did not achieve enough sensitivity.

Another broad absorption related to the conductive form of PPy (dication) appears at about 700 nm, and is also observed in the other three samples, which is in accordance to previously reported works [41]. In order to know the conductive behavior of our samples the band gap was calculated following the procedure described below.

The *band gap*, magnitude E_g, is the energy difference between the top of the valence band (HOMO, Highest Occupied Molecular Orbital) and the bottom of the conduction band (LUMO, Lowest Unoccupied Molecular Orbital) [42]. For this analyze, the procedures published by Botello *et al.* 2007 [43] and Brook *et al.* 2013 [40] were followed, the value of the intersection between line of best fit to the steepest part of the absorbance peak and the minimum absorbance observed for each sample was used in Planck equation that relate the energy of a photon and the frequency, according to the Equation 2.

$$E = hf \qquad \text{Eq. (2)}$$

where *E* is the energy (J), *h* Planck constant 6.6261×10^{-34} (J·s) and *f* frequency (Hz). Relating the frequency and speed of light we obtained the Equation 3.

$$\lambda = \frac{c}{f} \qquad \text{Eq. (3)}$$

where λ is the wavelength, *c* is the speed of light in vacuum. So the wavelength could be expressed as follow, Equation 4.

$$\lambda = \frac{hc}{E_g} \qquad \text{Eq. (4)}$$

where E_g is the energy of band gap and λ wavelength (m). Finally, the Equation 5 expresses separation energy in electron volts (eV) and the wavelength in nm.

$$E_g = \frac{1{,}24x10^3}{\lambda} \qquad \text{Eq. (5)}$$

Using the Equation 5 and the λ values obtained from Figure 18 (a,b,c and d), the band gap energy for each film was determined. The band gap results, which are given in in Table 6, indicate that all the polymers had a semiconductor behavior as was reported before [40] Besides, the PPy E_g turned out to be similar than the copolymers meaning that the introduction of a poor conductor (PEG) into the polymer chains has not been negative to its electrical performance.

Table 6: Wavelength of the highest absorption band corresponding to the π-π* transition band and band gap energies for all samples.

Sample	λ (nm)	E_g (eV)
PPy 300s	**551**	**2.25**
P(Py-*co*-PAB53) 300s	**539**	**2.30**
P(Py-*co*-PAB53) 500s	**547**	**2.27**
P(Py-*co*-PAB53) 1000s	**544**	**2.28**

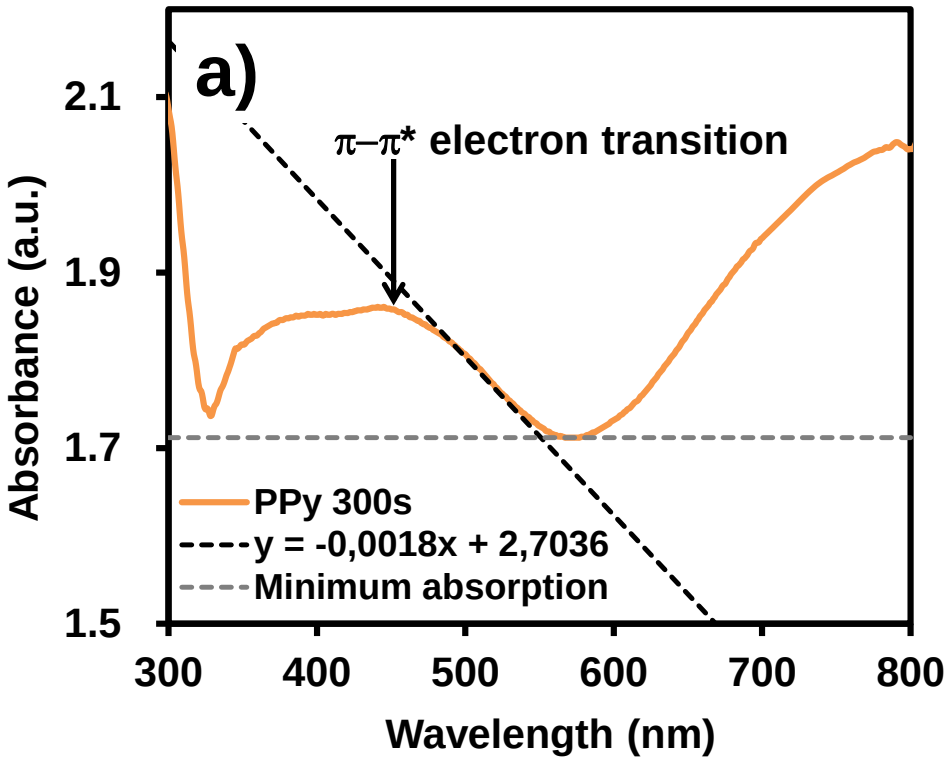
a)
π–π* electron transition
Absorbance (a.u.)
2.1
1.9
1.7
1.5
300
400
500
600
700
800
Wavelength (nm)
PPy 300s
y = -0,0018x + 2,7036
Minimum absorption

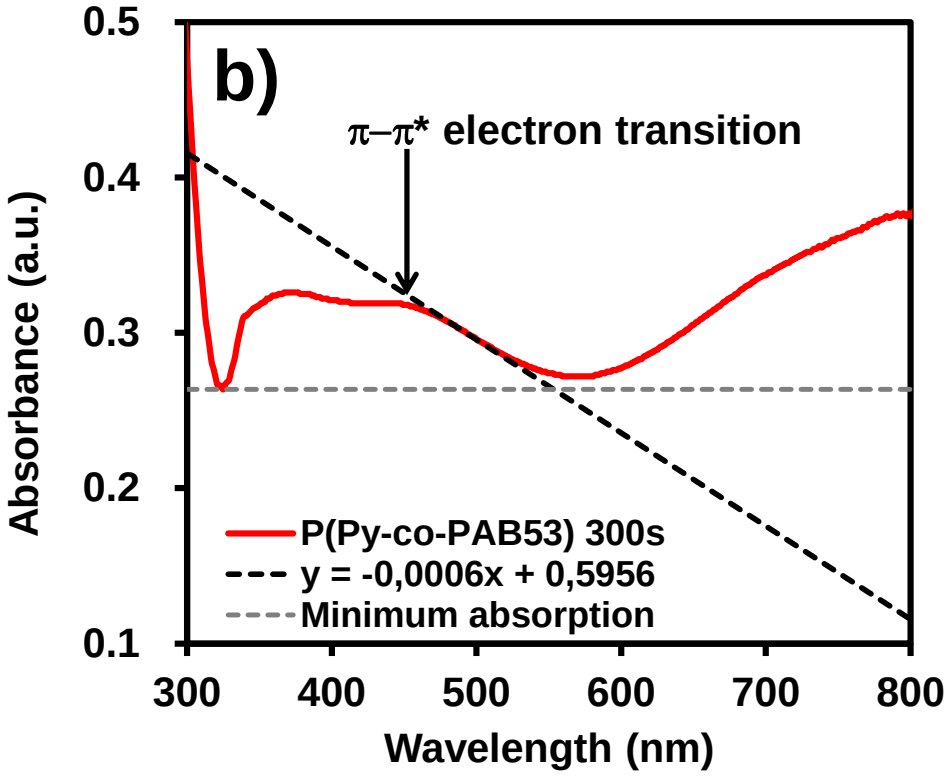
b)
π–π* electron transition
Absorbance (a.u.)
0.5
0.4
0.3
0.2
0.1
300
400
500
600
700
800
Wavelength (nm)
P(Py-co-PAB53) 300s
y = -0,0006x + 0,5956
Minimum absorption

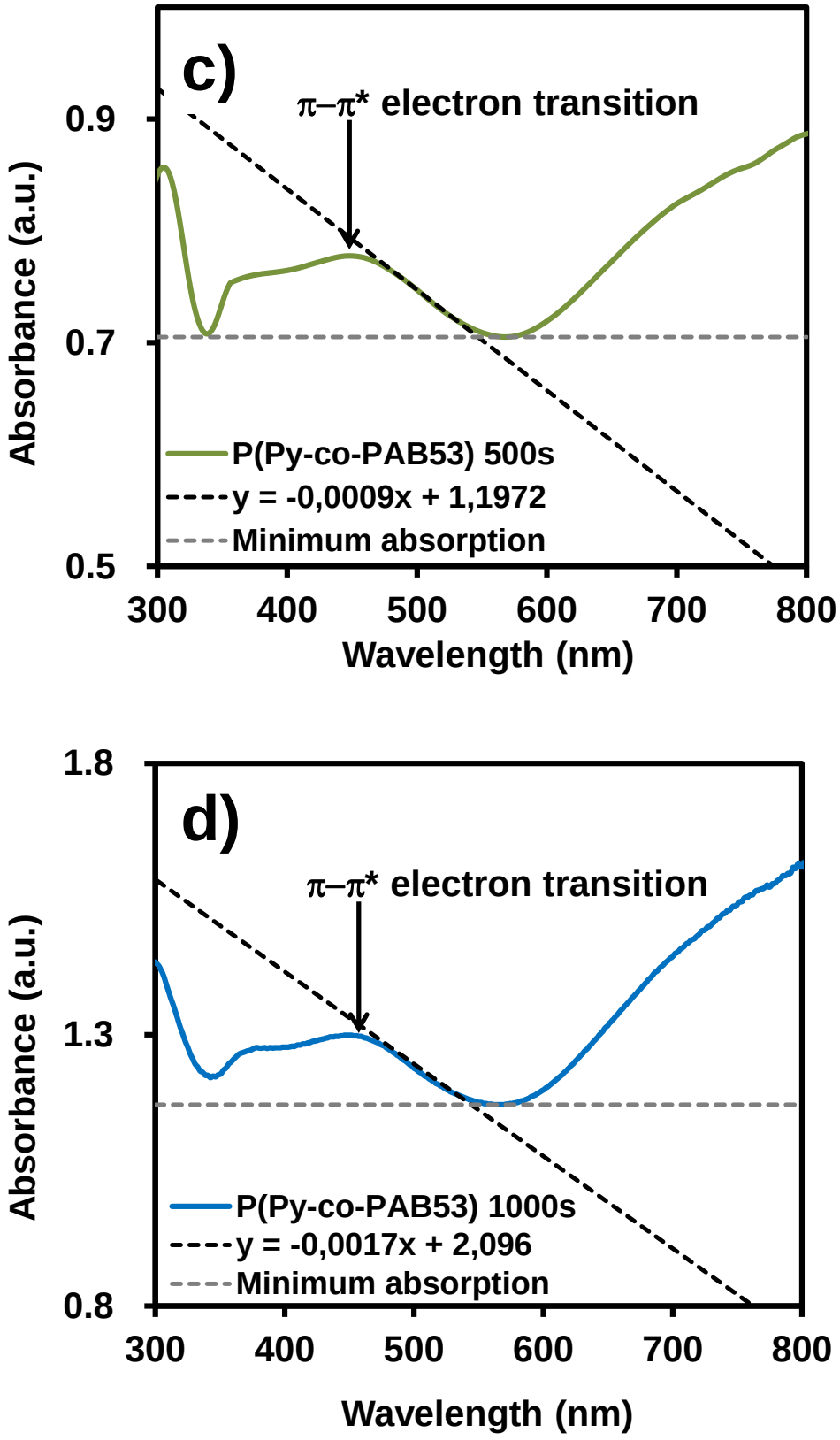

Figure 18: UV-vis spectra of (a) PPy homopolymer, (b) P(Py-co-PAB53) at 300s, (c) P(Py-co-PAB53) at 500s and (d) P(Py-co-PAB53) at 1000s The dotted lines represent the line of best fit used to determine the band gap (i.e. intersection of this line with the tangent.

4.7. Cellular adhesion

As Py:PAB53 (50:50) electropolymerized with 1000s at 1.6 V resulted to be the copolymer with the best film forming properties, it was the selected polymerization time used to generate several identical films to evaluated the proteins adsorption onto metal surface.

Adsorption is a nonspecific ubiquitous phenomenon mediated by non-specifics forces, for example electrostatic and hydrophobic interactions that affect a number of biotechnologies [9] [44]. Therefore, the proteins adsorbed onto the surface of the copolymer and PPy films were analyzed comparing them to the ones adsorbed onto steel surface (reference). The results are presented in the Figure 19.

As can be seen in both proteins, BSA and Lyz, the behavior was similar. Compared to the amount of proteins on the reference (steel surface), it was observed a decrease of 7% and 31%, BSA and Lyz respectively, on the PPy 300s surface. Opposite results were seen in the copolymer P(Py-*co*-PAB53) 1000s, which increasing was notorious (11% BSA and 29% Lyz). The increase on protein adsorption is intrinsically related to the presence of grafted PEG groups, that facilitates the interaction between the surface and the proteins. Another explanation is just related to the higher roughness and hydrophilicity of this copolymer compared to PPy homopolymer.

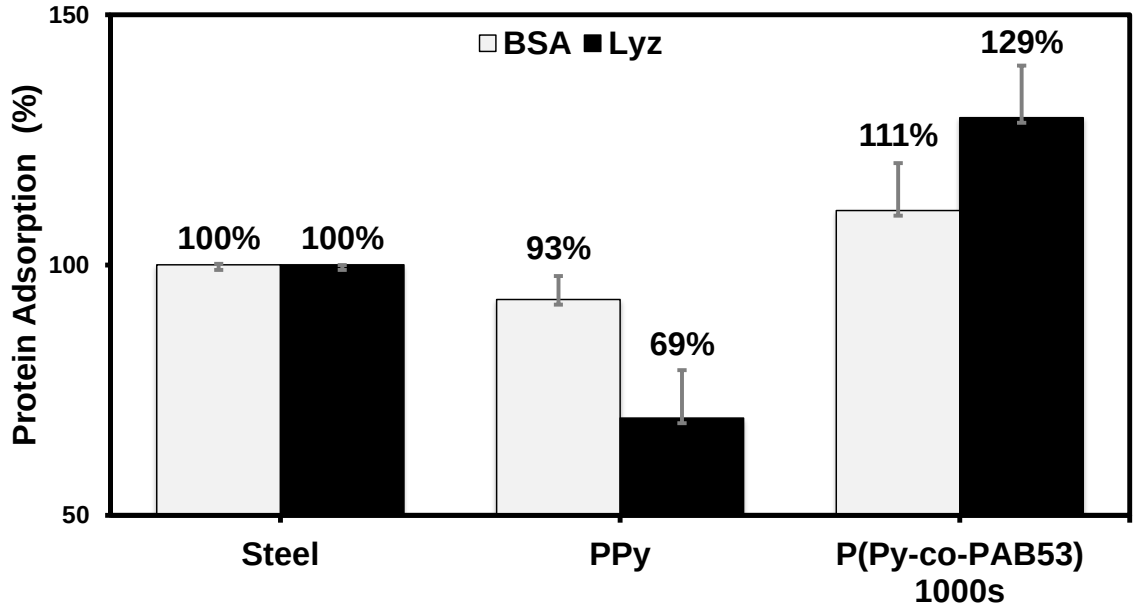

Figure 19: Adsorption of BSA and Lyz onto the surface of steel, PPy 300s and P(Py-*co*-PAB53) 1000s.

To corroborate the past absorption results, an electric field was applied to the proteins (previously extracted from the different surfaces *i.e.* steel, PPy 300s and the copolymer) with the purpose of make them migrate through a matrix of polyacrylamide.

One of the proteins used, the Bovine Serum Albumin, was depicted on Figure 20. In this image the three surfaces presented positive adsorption of BSA. However, the color intensity in the bands allowed us to confirm that the surface with lower affinity to this protein was the film of PPy, followed by steel and finally the copolymer generated at 1000s. Thus, the presence of PEG seems to be important for the biocompatibility of the copolymer, facilitating the adsorption of BSA onto its surface.

The other protein, Lysozyme, presented a similar electrophoretic response than BSA, with a major migration trough the gel due to its lower molecular weight [see Annex B].

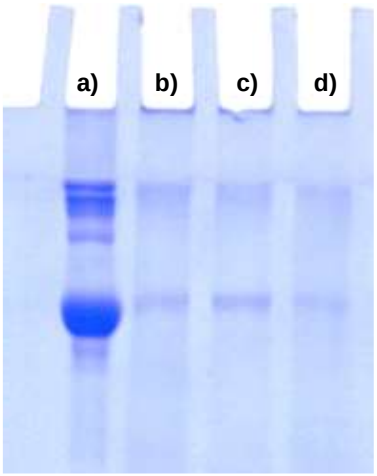

Figure 20: Electrophoresis gel of BSA results a) BSA (reference), b) steel, c) P(Py-co-PAB53) 1000s and d) PPy.

These results have shown that the biocompatibility of P(Py-*co*-PAB53) as actives surfaces for selective adsorption of specific proteins is higher than PPy homopolymer. Therefore, incorporation of hydrophilic backbone in conducting polymer chains is extremely important for future applications on the biological field.

However, several other proteins and also studies on cellular proliferation should be performed in a near future.

5. Temporary planning and costs

In this chapter is presented an economical evaluation of the project, to calculate the global cost have been classified the expenses as reagents and consumables, equipment, personnel and generals.

Reagents and consumables

The cost of each substance and consumables used during the phases of polymerization and characterizations can be seen in the Table 7 and 8. To obtain the final cost of each reagent was necessary apply a factor which corresponds to the fraction of unit used. In consumables case, was necessary indicated the number of units spent.

Table 7: Final cost of each reagent.

Product	Unit	Cost per unit (€)	Use factor	Final cost (€)
Acetonitrile	2000 mL	195.5	0.2500	48.90
$LiClO_4$	100 g	75.2	0.0480	3.60
Py	100 mL	70.7	0.0003	0.02
KBr	100 g	63.6	0.0200	1.30
$BaSO_4$	500 g	281.5	0.0100	2.80
BSA	5 g	286.0	0.1000	28.60
Lyz	25 g	718.0	0.0040	2.90
Tris	1000 g	65.4	0.0010	0.07
SDS	100 g	82.8	0.0500	4.10
BME	500 mL	23.4	0.0050	0.10
Acrylamide/Bis-acrylamide 30%	100 mL	42.9	0.3200	13.70
TEMED	100 mL	25.6	0.0050	0.10
Coomassie®	100 g	135.5	0.0030	0.40
Methanol	1000 mL	57.7	0.4000	23.10
Acetic acid	1000 mL	14.2	0.0500	0.70
Gel loading	5 mL	24.0	0.0600	1.40
Ninhydrin reagent	100 mL	67.1	0.1440	9.70
Total (€)				**141.50**

Table 8: Final cost of each consumable.

Product	Lot	Cost per lot (€)	Units used	Final cost (€)
Steel AISI 316L	625 mm^2	90.0	100 mm^2	14.4
ITO	10	349.0	1	34.9
Ag|AgCl electrode	1	136.1	1	136.1
Weighing Paper	500	35.9	15	1.1
Eppendorf Tubes	1000	36.3	90	3.3
Pipette tips 20 µL	960	72.9	25	1.9
Pipette tips 200 µL	960	68.8	70	5.0
Pipette tips 1000 µL	960	68.8	60	4.3
Total (€)				**201.0**

Equipment

The costs per hour of the equipment needed to perform the electropolymerizations and the different characterization are in Table 9. Some characterizations were performed in the CRnE with the internal UPC rate [45] [46].

Table 9: Costs per hour of the equipment used in this project.

Equipment	Time (h)	Cost (€/h)	Final Cost (€)
Potenciostate-galvanostat	15.0	35.0	525.0
FT-IR spectrophotometer *	5.0	5.1	25.7
Scanning electron microscope *	4.0	106.7	427.0
AFM Dimension microscope	10.0	31.7	317.4
Profilometer *	2.0	8.6	17.3
Contact angle meter	1.5	15.0	22.5
UV-Vis spectrophotometer *	4.0	4.9	19.4
Microplate reader	0.5	1.0	0.5
Total (€)			**1354.8**

(*): CRnE equipment.

Personnel

The labor cost was established based on the hours spent on the project and considering a minimum salary of 8 €/h [47], marked by the UPC practices agreement. The Table 10 shows the time inverted in the project and the associated cost.

Table 10: Associated cost of the hours inverted in the project.

Activity	Time (h)	Cost (€/h)	Final Cost (€)
Bibliographic research	110	8	880
Experimental test	460	8	3680
Results analysis	190	8	1520
Total (€)			**6080**

In general expenses were included electricity, water, basic lab and office material. To calculate it was estimated the 10% of the past expenses, resulting in 777.7 €. Thus the global cost of the project was 8 555 €, the final sum is shown in the Table 11.

Table 11: Global cost

Expense	Final cost (€)
Reagents	141.5
Consumables	201.0
Equipment	1354.8
Personnel	6080.0
Generals	777.7
Total (€)	**8555.0**

6. Environmental impact

This section describes a study of the possible environmental impact caused by the project carried out, following the recommendations published by González in 2011. She defines *environmental impact* as any action (activities, products or services) of an organization that transform or change directly or indirectly the environment, whether harmful or not. And the term *environmental* as all people, ecosystems, property, culture, socioeconomic structure… that are affected during the performance of a project [47].

This project is a preliminary stage of laboratory research, therefore, has been considered appropriate to include a section on the environmental impact during the experimental phase besides the possible impact generated by the copolymer P(Py-*co*-PAB53).

Environmental impact of experimental phase

To identify the impacts produce during the investigation, was necessary to understand that the cause of the on the environment impact is the activity and the consequence is the impact. This concept is explained in a better way in the Figure 21.

Figure 21: Scheme to identify environmental impacts

In concordance with the past concept and considering as main aspect use of chemical reagents, the principal impacts generated during experimental phase can be analyzed in the Figure 22. In order to prevent these effects was necessary: follow the normal lab safety rules (wear lab coats, gloves and protection glasses), store products and reagents in controlled atmospheres with proper ventilation and taking into account supplier's recommendations. Finally manage properly the waste produced, the company in charge of

this management was EcoCat, guidelines followed for classification and separations of waste are available online [49] [50] [51].

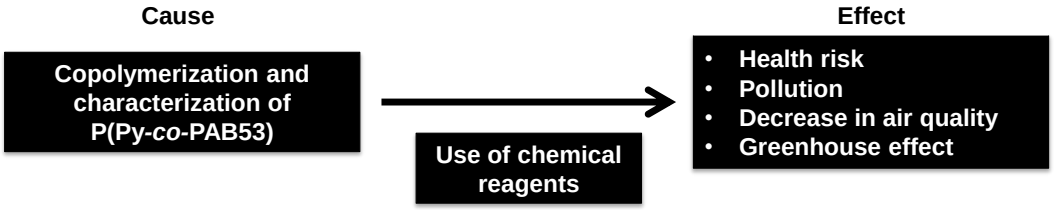

Figure 22: Causes and effects produced during this investigation.

Environmental impact of P(Py-*co*-PAB53)

This project is based on a research study that is not applicable on an industrial scale. Therefore, it was not possible to evaluate the environmental impact of its possible application. On the other hand, it is feasible to think that the compounds generated would not have a negative social and environmental impact, because it can contribute as a possible bioactive platform for medical devices and the PEG chains grafted on the backbone are biodegradable.

7. Conclusions

The present work looked for a methodology to obtain an electroactive biomaterial, based on a pyrrole backbone with chains of PEG_{2000} grafted in order to be able to use it as bioactive platforms for engineering applications. By electrochemical polymerization, at different polymerization time, it was found that it is possible to obtain a copolymer film in only 5 minutes. To corroborate the chemical structure of the films FTIR technique was used. The spectra showed characteristics peaks of PPy and PAB53 confirming that the films studied were generated correctly.

On the other hand, it was found that the morphology of the copolymers was similar, in all cases, to PPy homopolymer, *i.e.* cauliflower-like structures. Additionally, the topography and thickness were influenced by the polimerization time, even though the concentration of Py: PAB53 (50:50) was the same for the three times studied (300, 500 and 1000s). This factor affects the amount of material adhered onto the substrate. With longer polymerization times the metal substrate was completely covered and the concentration of PAB53 monomer in the copolymer films increased, as well the roughness and thickness.

The effect produced by the incorporation of PEG chains was traduced in a higher hydrophilicity than the homopolymer without PEG. Therefore, it improved the liquid-absorption properties of the materials, and also increased the roughness, which allows that the water penetrates into grooves formed. The water contact angles (θ) displayed to values lower than 90°. Another impact of the incorporation of PEG was observed on the electroactivity of the materials, the length of the chain hindered the optimum charge mobility across the copolymer chains causing a negative effect. However, the presence of PEG chains in the copolymer film does not decrease their ability to store charge.

Ultraviolet–visible spectroscopy reveals that the copolymers films exhibited a characteristic absorbance associated with π–π^* electron transition of conjugated PPy rings, besides, indicates that all the polymers had a semiconductor behavior, even with the incorporation of an isolating chain like PEG. This graft chain clearly improved the affinity of the copolymer P(Py-*co*-PAB53) generated at 1000s with the globular proteins BSA and Lyz in 11% and 29%, respectively. These results suggest that the P(Py-*co*-PAB53) is a promising system to explore for biotechnological applications. It would be necessary to

study other kind of proteins, antibacterial or antitumor cells different than that approached here to extend the biocompatibility study.

References

[1] R. Samatham, K. Kim, D. Dogruer, H. Choi, M. Konyo, M. J.D, Y. Nakabo, J. Nam, J. Su, S. Tadokoro, W. Yim and M. Yamakita, *Active Polymers: An Overview, in Electroactive Polymers for Robotic Applications: Artificial Muscles and Sensors*, Reno, NV: Springer Science & Business Editorial, 2007.

[2] K. Modjarrad and S. Ebnesajjad, *Handbook of Polymer Applications in Medicine and Medical Devices*, San Diego, CA: Elsevier Editorial, 2013.

[3] Y. Bar-Cohen, *Electroactive Polymers as Artificial Muscles – Reality and Challenges,* Seattle, WA: Structures, Structural Dynamics, and Materials Conference (SDM), 2001.

[4] G. Stienen, *Applications of Electroactive Polymers*, Roma, Italia: Springer Science & Business Media, 2012.

[5] M. Otake, *Electroactive Polymer Gel Robots: Modelling and Control of Artificial Muscles*, Chennai, India: Springer Science & Business Media, 2010.

[6] D. J. Leo, *Engineering Analysis of Smart Material Systems*, Blacksburg, VA: John Wiley & Sons Publication, 2007.

[7] H. Shirakawa, E. Louis, A. MacDiarmid, C. Chiang and A. Heeger, *Handbook of Conducting Polymers*, Boca Ratón, FL: Taylor & Francis Group, 2007.

[8] F. Wolfart, D. P. Dubal, M. Vidotti, R. Holze and P. Gómez-Romero, *Electrochemical supercapacitive properties of polypyrrole thin films: influence of the electropolymerization methods*, Journal of Solid State Electrochem, 2015.

[9] A.-D. Bendrea, G. Fabregat, J. Torras, S. Maione, L. Cianga, L. J. Del Valle, I. Cianga and C. Alemán, *Polythiophene-g-poly(ethylene glycol) graft copolymers for electroactive scaffolds*, Journal of Materials Chemistry B, 1, pp. 4135-4145, 2013.

[10] J. D. W. Madden, N. A. Vandesteeg, P. A. Anquetil, M. P. G. A., A. Takshi, R. Z. Pytel, S. R. Lafontaine, P. A. Wieringa and I. W. Hunter, *Artificial Muscle Technology:*

Physical Principles and Naval Prospects, IEEE Journal of Oceanic Engineering, 29 (30), pp. 706-728, 2004.

[11] C. Alemán, J. Casanovas, J. Torras, O. Bertrán, E. Armelin, R. Oliver and F. Estrany, *Cross-linking in polypyrrole and poly(N-methylpyrrole): Comparative experimental and theoretical studies*, J. Polymer, 49, pp. 1066-1075, 2008.

[12] G. Fabregat, C. Alemán, M. T. Casas and E. Armelin, *Controlling the Morphology of Poly(N-cyanoethylpyrrole),* The Journal of Physical Chemistry, 116, pp. 5064-5070, 2012.

[13] S. Zhong, Y. Zhang and C. Teck Lim, *Fabrication of Large Pores in Electrospun Nanofibrous Scaffolds for Cellular Infiltration: A Review*, Tissue Engineering: Part B, 18 (2), pp. 77-87, 2012.

[14] C. Mangold, F. Wurm and H. Frey, *Functional PEG-based polymers with reactive groups via anionic ROP of tailor-made epoxides*, J. Polymer Chemistry, 3, pp. 1714-1721, 2012.

[15] V. Karagkiozaki and S. Logothetidis, *Horizons in Clinical Nanomedicine*, Boca Raton, FL: Pan Stanford Publishing, 2014.

[16] R. Narayan, *Biomedical Materials*, Chapel Hill, NC: Springer Science & Business Media, 2009.

[17] J. M. Anderson, *Biological Responses to Materials*, Annual Review of Materials Research, 31, pp. 81-110, 2001.

[18] H.-Y. Cheung, K.-T. Lau, T.-P. Lu and D. Hui, *A critical review on polymer-based bio-engineered materials for scaffold development*, J. Composites Part B: Engineering, 38, pp. 291-300, 2007.

[19] S. Zalipsky, *Chemistry of polyethylene glycol conjugates with biologically active molecules*, Advanced drug delivery reviews, 16, pp. 157-182, 1995.

[20] A.-D. Bendrea, G. Fabregat, L. Cianga, L. J. Del Valle, I. Cianga, C. Alemán and F. Estrany, *Hybrid materials consisting of an all-conjugated polythiophene backbone and grafted hydrophilic poly(ethylene glycol) chains*, J. Polymer Chemistry, 4, pp. 2709-2723, 2013.

[21] R. Balint, N. J. Cassidy and S. H. Cartmell, *Conductive polymers: Towards a smart biomaterial for tissue engineering*, Acta Biomaterialia, 10, pp. 1341-2353, 2014.

[22] D. S. Chakraborty, *Instrumentation of FT-IR and its herbal applications*, World Journal of Pharmacy and Pharmaceutical Sciences, 5 (3), pp. 498-505, 2016.

[23] J. Goldstein, *Scanning Electron Microscopy and X-Ray Microanalysis: A Text for Biologists, Materials Scientists, and Geologists*, New York, NY: Springer Science & Business Media, 2012.

[24] R. Galgoczy, P. Roca-CusachS and J. Alcara, *Atomic Force Microscopy*, John Wiley & Sons Publication, 2013.

[25] J. Chinnam, D. Das, R. Vajjha and J. Satti, *Measurements of the contact angle of nanofluids and development of a new correlation*, International Communications in Heat and Mass Transfer, 62, pp. 1-12, 2015.

[26] S. Bell, *Encyclopedia of Forensic Science*, New York, NY: Infobase Publishing, 2008.

[27] M. Friedman, *Applications of the Ninhydrin Reaction for Analysis of Amino Acids, Peptides, and Proteins to Agricultural and Biomedical Sciences*, Journal of Agricultural and Food Chemistry, 52, pp. 385-406, 2004.

[28] B. Hames, *Gel Electrophoresis of Proteins: A Practical Approach (3th ed.)*, Oxford, NY: Oxford University Press, 1998.

[29] M. M. Pérez-Madrigal, L. Cianga, L. J. Del Valle, I. Cianga and C. Alemán, *Electroactive and bioactive films of random copolymers containing terthiophene, carboxyl and Schiff base functionalities in the main chain*, J. Polymer Chemistry, 6, pp. 4319-4335, 2015.

[30] H. Eisazadeh, *Studying the Characteristics of Polypyrrole and its Composites*, World Journal of Chemistry, 2 (2), pp. 67-74, 2007.

[31] M. A. Chougule, S. G. Pawar, P. R. Godse, R. N. Mulik, S. Sen and V. B. Patil, *Synthesis and Characterization of Polypyrrole (PPy) Thin Films*, Soft Nanoscience Letters, 1, pp. 6-10, 2011.

[32] X. Yang, T. Dai, M. Wei and Y. Lu, *Polymerization of pyrrole on a polyelectrolyte hollow-capsule microreactor*, Polymer, 47, pp. 4596-4602, 2006.

[33] C. Mangeney, S. Bousalem, C. Connan, M.-J. Vaulay, S. Bernard and M. M. Chehimi, *Latex and Hollow Particles of Reactive Polypyrrole: Preparation, Properties, and Decoration by Gold Nanospheres*, Langmuir, 22, pp. 10163-10169, 2006.

[34] M. Catauro, R. Renella, F. Papale and S. Vecchio Ciprioty, *Investigation of bioactivity, biocompatibility and thermal behavior of sol–gel silica glass containing a high PEG percentage*, Materials Science and Engineering C, 61, pp. 51-55, 2016.

[35] D. Aradilla, F. Estrany, E. Armelin and C. Alemán, *Morphology and growing of nanometric multilayered films formed by alternated layers of poly(3,4-ethylenedioxythiophene) and poly(N-methylpyrrole),* Thin Solid Films Journal, 518, pp. 4203-4210, 2010.

[36] Siong Teh, Kwok; Takahashi, Yusuke; Yao, Zhonghua; Lu Yen-Wen, *Influence of redox-induced restructuring of polypyrrole on its surface morphology and wettability,* Sensors and Actuators A: Physical, 155 (1), pp. 113-119, 2009.

[37] T. Darmanin and F. Guittard, *Wettability of conducting polymers: From superhydrophilicity to superoleophobicity*, Progress in Polymer Science, 39 (4), pp. 656-682, 2014.

[38] R. N. Wenzel, *Resistance of solid surfaces to wetting by water*, Industrial and Engineering Chemistry, 28 (8), pp. 988-994, 1936.

[39] W. Hou, Y. Xiao, G. Han and H. Zhou, *Electro-polymerization of polypyrrole/multi-wall carbon nanotube counter electrodes for use in platinum-free dye-sensitized solar cells*, Electrochimica Acta, 190, pp. 720-728, 2016.

[40] R. Brooke, D. Evans, P. Hojati-Talemi, P. Murphy and M. Fabretto, *Enhancing the morphology and electrochromic stability of polypyrrole via PEG–PPG–PEG templating in vapour phase polymerisation*, European Polymer Journal, 51, pp. 28-36, 2014.

[41] F. Inoue, R. A. Ando, C. M. Izumi and P. Corio, *Spectroscopic Characterization of Carbon Nanotube-Polypyrrole Composites*, The Journal of Physical Chemistry C, 118, pp. 18240-18248, 2014.

[42] R. J. D. Tilley, *Colour and the Optical Properties of Materials: An Exploration of the Relationship Between Light, the Optical Properties of Materials and Colour (2th ed.)*, Noida, India: John Wiley & Sons Publication, 2010.

[43] L. A. Botello Salinas, M. T. Garza González, I. Gómez de la Fuente and M. Hinojosa Rivera, *Biosíntesis de nanopartículas de ZnS utilizando cepas de hongos*, J. Ingenierías, 10 (37), pp. 16-22, 2007.

[44] Y. Cai and D. K. Schwartz, *Influence of Protein Surface Coverage on Anomalously Strong Adsorption Sites*, Applied Materials and Interfaces, 8, pp. 511-520, 2016.

[45] CRNE., *Centre de Recerca en Nanoenginyeria. CRNE*., UPC-CRNE, [Online]. Available: https://www.upc.edu/crne/ca. [Accessed 1 07 2016].

[46] CRNE., *Centre de Recerca en Nanoenginyeria. CRNE. Infraestructura*, UPC-CRNE, [Online]. Available: https://www.upc.edu/crne/ca/infraestructura/serveis-i-tarifes [Accessed 1 07 2016].

[47] Facultat d'Informàtica de Barcelona, *Información para la empresa*, UPC- FIB, [Online]. Available: http://www.fib.upc.edu/es/empresa/practiques/empresa.html [Accessed 1 07 2016].

[48] M. González, *Consideraciones ambientales para los PFC*, Barcelona, España: Dpto. Proyectos de Ingeniería - UPC, 2011.

[49] Universitat Politècnica de Catalunya, *Prevencion de Riesgos Laborales*, UPC, [Online]. Available: https://www.upc.edu/prevencio/es/seguridad-e-higiene/recogida-de-residuos [Accessed 1 07 2016].

[50] Universitat Politècnica de Catalunya, *Recursos i Serveis per a la Gestió Sostenible,* UPC, [Online]. Available: https://www.upc.edu/gestiosostenible/residus/recollida-selectiva/gestio-de-residus-de-laboratori/gestio-de-residus-de-laboratori [Accessed 1 07 2016].

[51] Universitat Politècnica de Catalunya, *Recursos i Serveis per a la Gestió Sistenible-Ecocat*, UPC-Ecocat, [Online]. Available: https://www.upc.edu/gestiosostenible/residus/recollida-selectiva/gestio-de-residus-de-

laboratori/com-hem-de-gestionar-els-residus-de-laboratori/proces-recollida-de-residus-de-laboratori/tractament-final-dels-residus/ecocat [Accessed 1 07 2016].

Complementary

- G. Fabregat Jové, *Conducting polymers and hybrid derivatives with specific applications as sensors and bioative platforms*, Barcelona, España: Universitat Politècnica de Catalunya, PhD thesis, 2014.

- E. Redondo Negrete, *Synthesis of functionalized polythiophenes for detection of biomolecules*, Barcelona, España: Escola Tècnica Superior d´Enginyeria Industrial de Barcelona, Master thesis, 2013.